AGU PUBLICATIONS

Paleoceanography

RESEARCH ARTICLE
10.1002/2015PA002793

Key Points:
- *E. rex* utilized dissolved silicon mainly from Asian dust during the LGM
- Surface waters of the EPS were eutrophic for dissolved silicon during the LGM
- A new model for formation of laminated diatom mats by *E. rex* is developed

Correspondence to:
T. Li,
tgli@qdio.ac.cn

Citation:
Xiong, Z., et al. (2015), The silicon isotope composition of *Ethmodiscus rex* laminated diatom mats from the tropical West Pacific: Implications for silicate cycling during the Last Glacial Maximum, *Paleoceanography*, *30*, 803–823, doi:10.1002/2015PA002793.

Received 17 FEB 2015
Accepted 21 MAY 2015
Accepted article online 26 MAY 2015
Published online 6 JULY 2015

The silicon isotope composition of *Ethmodiscus rex* laminated diatom mats from the tropical West Pacific: Implications for silicate cycling during the Last Glacial Maximum

Zhifang Xiong[1], Tiegang Li[1], Thomas Algeo[2,3], Kristin Doering[4,5], Martin Frank[5], Mark A. Brzezinski[6], Fengming Chang[1], Sophie Opfergelt[7], Xavier Crosta[8], Fuqing Jiang[1], Shiming Wan[1], and Bin Zhai[9]

[1]Key Laboratory of Marine Geology and Environment, Institute of Oceanology, Chinese Academy of Sciences, Qingdao, China, [2]Department of Geology, University of Cincinnati, Cincinnati, Ohio, USA, [3]State Key Laboratories of Biogeology and Environmental Geology, and Geological Processes and Mineral Resources, China University of Geosciences, Wuhan, China, [4]Institute of Geosciences, University of Kiel, Kiel, Germany, [5]GEOMAR Helmholtz Centre for Ocean Research Kiel, Kiel, Germany, [6]Marine Science Institute and Department of Ecology, Evolution and Marine Biology, University of California, Santa Barbara, California, USA, [7]Earth and Life Institute, Université catholique de Louvain, Louvain-la-Neuve, Belgium, [8]UMR-CNRS 5805 EPOC, Université de Bordeaux, Allée Geoffroy Saint Hilaire, Pessac CEDEX, France, [9]Key Laboratory of Marine Hydrocarbon Resource and Geology, Qingdao Institute of Marine Geology, Ministry of Land and Resources, Qingdao, China

Abstract The cause of massive blooms of *Ethmodiscus rex* laminated diatom mats (LDMs) in the eastern Philippine Sea (EPS) during the Last Glacial Maximum (LGM) remains uncertain. In order to better understand the mechanism of formation of *E. rex* LDMs from the perspective of dissolved silicon (DSi) utilization, we determined the silicon isotopic composition of single *E. rex* diatom frustules ($\delta^{30}Si_{E.\ rex}$) from two sediment cores in the Parece Vela Basin of the EPS. In the study cores, $\delta^{30}Si_{E.\ rex}$ varies from −1.23‰ to −0.83‰ (average −1.04‰), a range that is atypical of marine diatom $\delta^{30}Si$ and that corresponds to the lower limit of reported diatom $\delta^{30}Si$ values of any age. A binary mixing model (upwelled silicon versus eolian silicon) accounting for silicon isotopic fractionation during DSi uptake by diatoms was constructed. The binary mixing model demonstrates that *E. rex* dominantly utilized DSi from eolian sources (i.e., Asian dust) with only minor contributions from upwelled seawater sources (i.e., advected from Subantarctic Mode Water, Antarctic Intermediate Water, or North Pacific Intermediate Water). *E. rex* utilized only ~24% of available DSi, indicating that surface waters of the EPS were eutrophic with respect to silicon during the LGM. Our results suggest that giant diatoms did not always use a buoyancy strategy to obtain nutrients from the deep nutrient pool, thus revising previously proposed models for the formation of *E. rex* LDMs.

1. Introduction

As a typical giant diatom species, *Ethmodiscus rex* shows distinct physiological and ecological features that distinguish it from small spring-bloom diatoms. Compared with cell volumes of 10^3–10^5 μm^3 for spring-bloom diatoms, *E. rex* has much large cell volumes (up to 10^9 μm^3) dominated by a single vacuole (>99% of total volume) [*Villareal et al.*, 1999a, 2007]. Whereas spring-bloom diatoms favor well-mixed, fertile surface waters, *E. rex* reaches maximum abundance within stable and stratified, oligotrophic water masses [*Villareal et al.*, 1999a; *Kemp et al.*, 2000]. To overcome the nutrient deficiency of surface waters, *E. rex* commonly utilizes a buoyancy strategy of migrating vertically between the surface for photosynthesis and the nutricline to obtain nutrients, e.g., dissolved silicon (DSi), nitrate, and phosphate [*Villareal*, 1992; *Villareal and Carpenter*, 1994; *Kemp et al.*, 2006]. In addition, giant diatoms can utilize nutrient inputs resulting from episodic breakdown of the thermocline [*Goldman*, 1993; *Goldman and McGillicuddy*, 2003] or tap into the nutrient pool via symbiosis with nitrogen-fixing cyanobacteria [*Villareal*, 1991; *Carpenter et al.*, 1999]. Relying on abundant DSi and nitrate trapped in deep nutrient pools, *E. rex* can sustain blooms lasting several months from early summer to late fall [*Kemp et al.*, 2000, 2006]. The long duration of *E. rex* blooms generates total primary production that rivals or exceeds that of small-diatom blooms, which generally last from several days to a few weeks in the spring [*Kemp et al.*, 2000]. However, the growth and production rates of *E. rex* are substantially lower than those of spring-bloom diatoms [*Kemp et al.*, 2000]. Once seasonal mixing breaks down water column stratification,

E. rex blooms subside, resulting in a massive flux of diatom biomass to the deep ocean, where it rapidly accumulates on the seafloor as laminated diatom mats (LDMs).

Due to the rare occurrence of *E. rex* in the modern global ocean and its unusual ecology, the formation of LDMs is still not well understood—a situation that has been referred to as the "*E. rex* problem" [*Gardner and Burckle*, 1975; *Abrantes*, 2001]. Several mechanisms have been proposed for the formation of *E. rex* LDMs in different oceanic regions (see review in *Romero and Schmieder* [2006]). In their seminal taxonomic study of LDMs from the Mariana Ridge-Trough-Trench region, *Wiseman and Hendey* [1953] inferred massive, short-duration blooms of *E. rex*. This explanation was further elaborated in the "strong-upwelling-plus-intense-bloom" hypothesis, according to which upwelling supplies *E. rex* with episodic pulses of nutrients [*Gardner and Burckle*, 1975; *Stabell*, 1986; *Abrantes*, 2001]. However, the general use of *E. rex* as a paleo-upwelling indicator is not warranted because modern studies of its ecology have shown that upwelling is not a necessary condition for *E. rex* blooms [*Villareal et al.*, 1999a]. An alternative, the "differential dissolution" hypothesis, proposed that strong dissolution of other diatom species together with minimal dissolution of *E. rex* due to its rapid sinking and short exposure time to seawater favored its relative enrichment in the sediment [*Bukry*, 1974; *Schrader*, 1974; *Mikkelsen*, 1977]. Also, several investigations have suggested that local seafloor bathymetry plays a critical role in the formation of *E. rex* LDMs. For example, *Gombos* [1984] pointed out that preservation of *E. rex* LDMs may have been promoted within a closed depression on the Mid-Atlantic Ridge having poor bottom circulation and reduced dissolved O_2 levels. Nevertheless, these mechanisms either apply exclusively to a particular oceanic region or seek only to explain the accumulation of *E. rex* LDMs rather than the underlying causes of *E. rex* blooms.

Recent advances in our knowledge of the ecology and biochemistry of *E. rex* [*Villareal*, 1992; *Villareal and Carpenter*, 1994; *Villareal et al.*, 1999a, 2007] have yielded two new models for the formation of giant diatom LDMs. In the "ocean stratification model," *E. rex* blooms develop within a deep chlorophyll maximum layer under stratified conditions and utilize a buoyancy strategy of vertical migration between the ocean surface for photosynthesis and the nutricline to obtain nutrients [*Villareal et al.*, 1999a; *Kemp et al.*, 2000, 2006]. In the "frontal zone model," *E. rex* congregates along an oceanic front, first taking up nutrients and growing in cold upwelling waters beneath the frontal boundary and then ascending into overlying warm oligotrophic waters by regulated buoyancy [*Yoder et al.*, 1994; *Kemp et al.*, 2006]. Because these models take into consideration the unusual ecological characteristics of *E. rex* (i.e., its buoyancy strategy and association with oligotrophic conditions), they are now widely accepted as the most likely mechanisms of formation of *E. rex* LDMs. Each model has regional applicability: strong oceanic stratification is linked to *E. rex* blooms in the tropical ocean [e.g., *Gingele and Schmieder*, 2001; *De Deckker and Gingele*, 2002; *Kemp and Villareal*, 2013] and frontal zones to blooms in subtropical settings [e.g., *Pike*, 2000; *Kemp et al.*, 2010; *Rackebrandt et al.*, 2011]. Both models invoke deep nutrient pools for *E. rex* blooms, raising the question of whether all nutrients utilized by *E. rex* are taken from such pools. Studies of giant diatoms have provided unambiguous evidence of nitrate uptake from deep nutrient pools [*Villareal et al.*, 1993, 1999b]. However, the source of the nutrient DSi used in biomineralization has not been unambiguously determined to date, although significant surface DSi uptake by *E. rex* has been reported [*Villareal et al.*, 1999a].

The silicon isotopic composition of diatom opal ($\delta^{30}Si_{diatom}$) has great potential for tracing DSi utilization by diatoms in paleoceanographic and paleolimnological investigations (see reviews in *De La Rocha* [2006], *Crosta and Koç* [2007], and *Leng et al.* [2009]). Diatoms preferentially assimilate the light isotope of silicon (^{28}Si) when they take up DSi from ocean-surface waters for frustule formation, thus leaving the nutrient pool enriched in the heavy isotope of silicon (^{30}Si). As the nutrient pool becomes enriched in ^{30}Si, this signal is also transferred to diatom opal [*De La Rocha et al.*, 1997]. Thus, increased $\delta^{30}Si_{diatom}$ is generally indicative of greater degrees of DSi utilization in ocean-surface waters. The silicon isotopic fractionation factor associated with DSi uptake is thought to be essentially constant ($^{30}\varepsilon = -1.1‰$) and independent of temperature and growth rates [*De La Rocha et al.*, 1997], pH [*Milligan et al.*, 2004], salinity [*Alleman et al.*, 2005], and cell size [*Cardinal et al.*, 2007], although species-specific effects have been discovered recently [*Sutton et al.*, 2013] (see section 4.3.1). The utility of silicon isotopes for analysis of silica biomineralization has been further confirmed through a series of studies that have quantified diatom growth and its effect on the DSi pool in modern aqueous systems [*De La Rocha et al.*, 2000, 2011; *Varela et al.*, 2004; *Cardinal et al.*, 2005, 2007; *Beucher et al.*, 2008, 2011; *Fripiat et al.*, 2011a, 2011b, 2012; *Cao et al.*, 2012; *de Souza et al.*, 2012a, 2012b; *Ehlert et al.*, 2012;

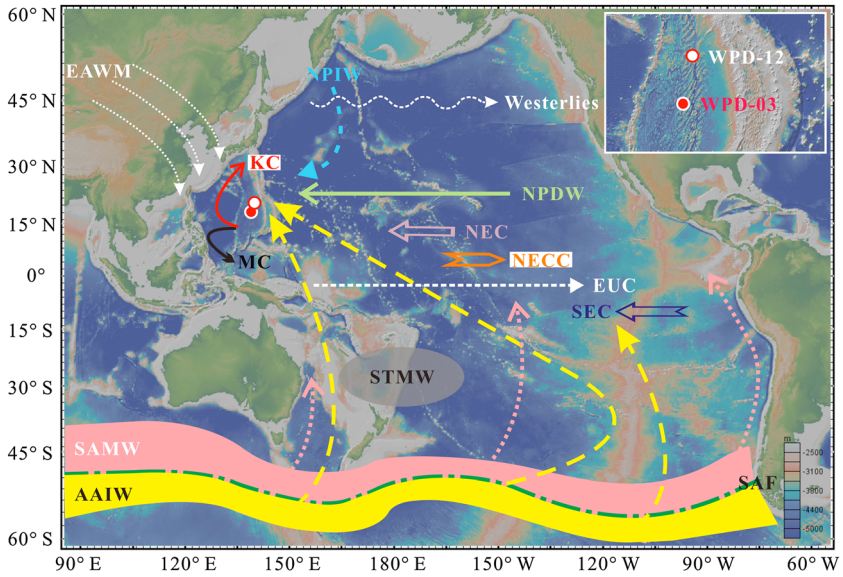

Figure 1. Map of the tropical West Pacific showing the locations of cores WPD-03 and WPD-12, regional ocean circulation (modified from *Fine et al.* [1994], *Siedler et al.* [2004], *Bostock et al.* [2010], *Kawabe and Fujio* [2010], and *Rose et al.* [2010]), and schematic Asian dust trajectories (modified after *Nilson and Lehmkuhl* [2001], *Shao et al.* [2011], and *Muhs* [2013]). Abbreviations: AAIW, Antarctic Intermediate Water; EAWM, East Asian winter monsoon; EUC, Equatorial Undercurrent; KC, Kuroshio Current; MC, Mindanao Current; NEC, North Equatorial Current; NECC, North Equatorial Counter Current; NPDW, North Pacific Deep Water; NPIW, North Pacific Intermediate Water; SAF, Subantarctic Front; SAMW, Subantarctic Mode Water; SEC, South Equatorial Current; and STMW, Subtropical Mode Water. The map is a Mercator projection drawn using the online map generator at http://www.geomapapp.org/MSInstall.html.

Grasse et al., 2013; *Singh et al.*, 2015]. However, most of these studies utilized mixed-species $\delta^{30}Si_{diatom}$ records from polar-ocean sediments, making the broader applicability of their conclusions uncertain.

E. rex LDMs were deposited widely in the eastern Philippine Sea (EPS) during the Last Glacial Maximum (LGM) [*Xiong et al.*, 2013a, and references therein], as documented in a series of cores recovered from the Parece Vela Basin (Figure 1) during the 2003–2004 cruise of R/V *Science No. 1* [*Zhai et al.*, 2009]. The widespread occurrence of *E. rex* LDMs in the EPS during the LGM is puzzling. First, the modern EPS is characterized by oligotrophic and low-productivity surface waters having silicate and chlorophyll *a* concentrations of just 2.5–3.5 $\mu mol\,L^{-1}$ and 0.04–0.07 $mg\,m^{-3}$, respectively (Figures 2a–2c). However, DSi availability during the LGM may have been much greater than at present, which raises two important questions. What was the source of DSi for *E. rex* blooms during the LGM? And what was the degree of DSi utilization by *E. rex*? Second, the EPS is located on the northern margin of the Western Pacific Warm Pool, which is modulated by large-scale climatic patterns linked to the El Niño–Southern Oscillation [*Chiang*, 2009]. In this area, El Niño-like conditions led to shoaling of the thermocline during the LGM and, thus, to increased nutrient inputs to the surface waters [*Stott et al.*, 2002]. However, greater vertical mixing and turbulence during the LGM should have served to repress *E. rex* blooms, raising additional important questions. What was the trigger for these *E. rex* blooms? Were *E. rex* blooms linked to vertical mixing events or to other proximate causes? In order to answer these questions, we present the first $\delta^{30}Si_{diatom}$ records from two tropical-ocean cores containing *E. rex* LDMs. The results of this study not only allow reconstruction of the DSi state of the EPS during the LGM but also provide new insights concerning the formation of *E. rex* LDMs.

2. Materials and Methods

2.1. Core Descriptions and Age Models

E. rex LDMs were analyzed for $\delta^{30}Si_{diatom}$ in two deep-sea cores from the Parece Vela Basin of the EPS (Figure 1): (1) core WPD-03, 405 cm long, recovered during the 2004 cruise of R/V *Science No. 1* in 5250 m water depth at 17°19.82′N and 138°27.28′E, and (2) core WPD-12, 100 cm long, obtained during the 2003 cruise of R/V *Science No. 1* in 4954 m water depth at 20°35.95′N and 139°14.54′E. Both of the cores contain

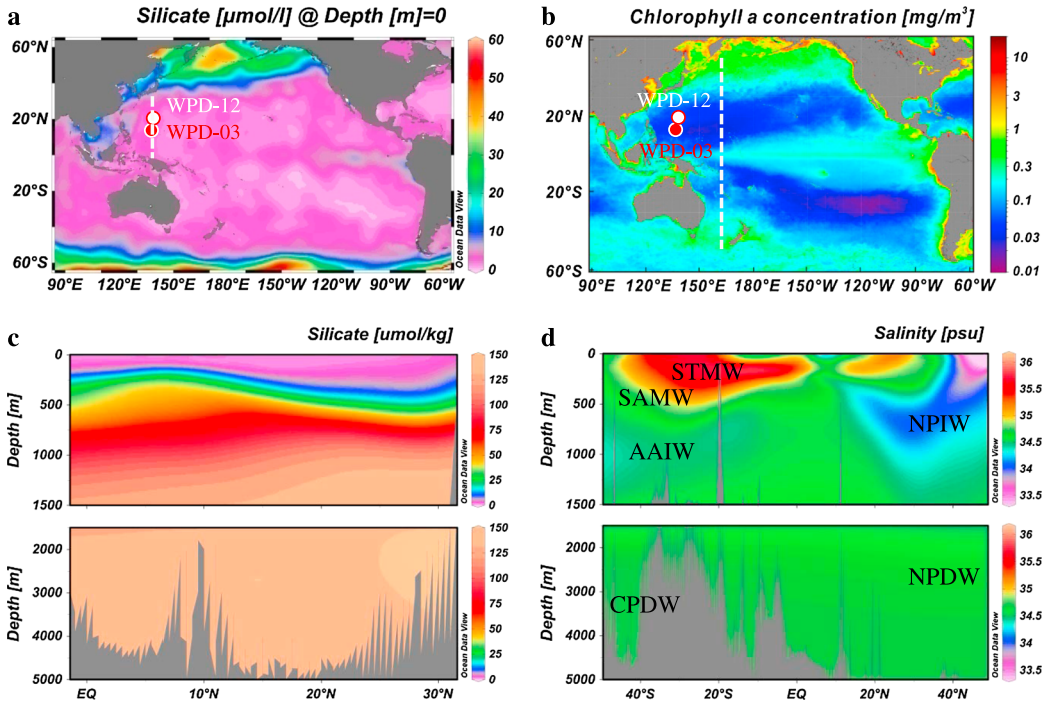

Figure 2. Maps of annual mean surface (a) silicate and (b) chlorophyll *a* concentrations in the tropical West Pacific. Latitudinal depth sections of (c) silicate concentrations along 139°E (i.e., close to the study cores) and (d) salinity along 163°E. In Figure 2d, CPDW is Circumpolar Deep Water; see Figure 1 for other abbreviations. Figures 2a, 2c, and 2d were generated using the Ocean Data View software (http://www.odv.awi.de) [*Schlitzer*, 2000], and Figure 2b was developed from SeaWiFS satellite imagery (http://www.oceancolor.gsfc.nasa.gov/cgi/l3). The white dashed lines in Figures 2a and 2b show the locations of the cross sections in Figures 2c and 2d, respectively.

little carbonate (<1%) because the study sites lie below the calcium carbonate compensation depth [*Xiong et al.*, 2012b]. The longer core (WPD-03) comprises three discrete lithostratigraphic units. The upper unit (0–286 cm; all depths are relative to the core top) is composed of olive-grey and grey, laminated diatom mats (LDM-03), which are dominated by fragmented valves of the mat-forming diatom *E. rex* in near-monospecific assemblages (Figure 3a) with extremely low abundances of other diatom species and radiolarians (Figure 3b) [*Zhai et al.*, 2009]. The middle unit (286–334 cm) is characterized by grey diatomaceous clays (DCs) that are dominated by *E. rex* and small spring-bloom diatoms [*Zhai et al.*, 2012] but lack lamination. The lower unit (334–405 cm) comprises massive red pelagic clays (PCs) that generally lack a microfossil component. The shorter core (WPD-12) contains only the laminated diatom mat facies (LDM-12), which resembles that of LDM-03 but contains greater quantities of nonbiogenic silica.

The construction of an age model for core WPD-03 was based on linear regression of the calibrated radiocarbon age data (see details in *Xiong et al.* [2013a]). This model dates deposition of the DC and LDM-03 units to 31.0–29.4 kyr and 29.4–19.5 kyr, respectively (note that all reported ages are "before present") [*Xiong et al.*, 2013a]. Unfortunately, the age model of core WPD-12 is not well established due to reversed accelerator mass spectrometry (AMS)^{14}C age data throughout the core, and the age of the cored interval can be constrained only broadly to between ~25 kyr and ~19 kyr [*Zhai et al.*, 2009]. Possible reasons for AMS^{14}C age reversals in the study cores were considered by *Xiong et al.* [2013a]. Post-LGM sediments are missing at the tops of the study cores due to coring-induced loss of a thin (<~3 cm) fluff layer that represents the limited accumulation of pelagic clays in the EPS since ~19 kyr, which is an interval without LDM formation.

2.2. Diatom Extraction and Silicon Isotope Analysis

A series of physical separation and chemical oxidation steps were utilized to extract and isolate diatoms, including the primary species of interest (*E. rex*), for silicon isotope measurements [*Xiong et al.*, 2012c]. Bulk wet samples (Figure 3a) were treated with 10% H_2O_2 and 1 mol mL^{-1} HCl to remove excess organic matter and carbonate. The samples were then wet sieved to obtain the 63–154 µm and >154 µm size fractions

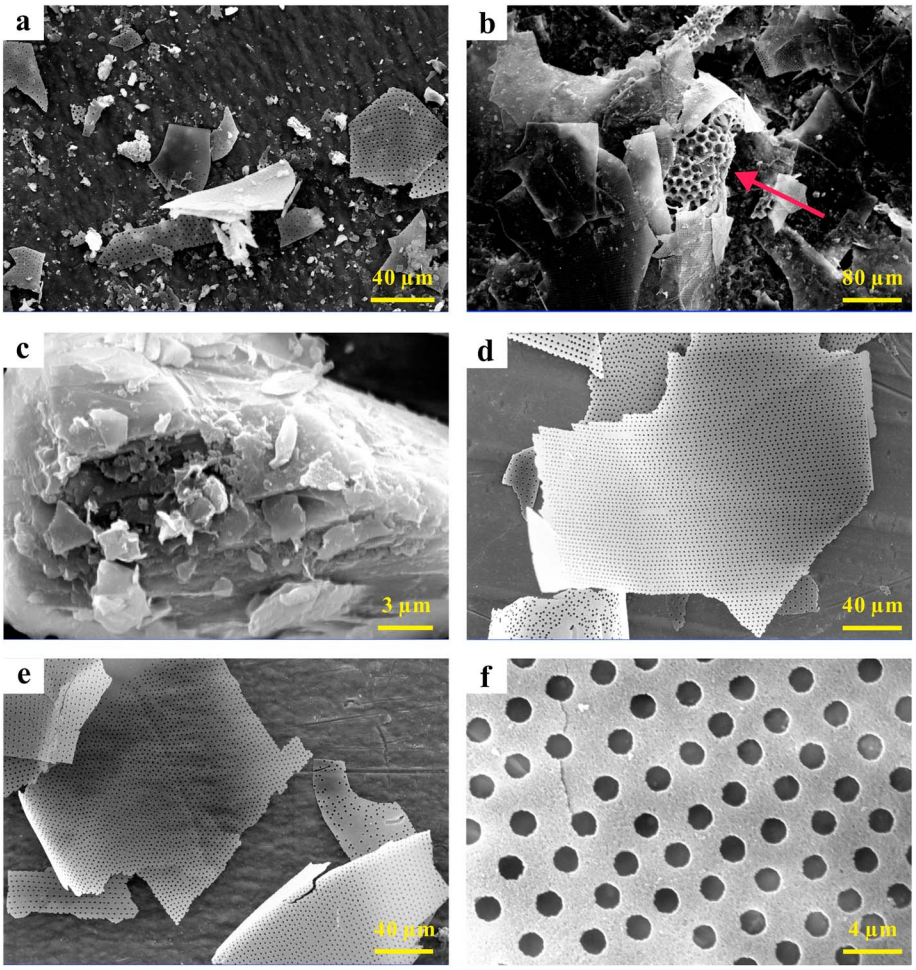

Figure 3. Scanning electron microscope photos showing samples before and after cleaning for silicon isotope analysis. (a) Bulk sediment sample before physical separation, (b) radiolarian (marked by the red arrow) in sample before physical separation, (c) detrital grain in sample before physical separation, (d) >154 µm *E. rex* frustules after physical separation, (e) 63–154 µm *E. rex* frustules after physical separation, and (f) pure *E. rex* frustules following removal of labile organic matter by chemical oxidation.

using 63 µm and 154 µm steel meshes. Pure diatom remains were obtained from the two size fractions via centrifugation at 1500 rpm and heavy liquid flotation using 2.3 g mL^{-1} sodium polytungstate (Figures 3d and 3e). Labile organic matter coating the diatom frustules was removed via a chemical oxidation step, in which samples were immersed in 30% H_2O_2 at 65°C for 2 h. Sample purity was verified by visual inspection of treated samples using both standard light and scanning electron (SEM) microscopy. The 63–154 µm and >154 µm diatom fractions consist of nearly pure *E. rex* except for the presence of trace radiolarians (<3%) in the 63–154 µm fraction [*Xiong et al.*, 2013a]. However, our experiments indicate that samples with opal concentrations of <10% cannot be totally purified by the physical separation technique described here [*Xiong et al.*, 2012c].

The cleaned >154 µm *E. rex* fractions (Figure 3f) were used for silicon isotopic measurements. About 75 µL of the *E. rex* samples were transferred into Teflon vials, dried and dissolved in 1 mL 0.1 mol L^{-1} NaOH at 130°C for 24 h. Residual detrital material was separated afterward via centrifugation, and traces of organic matter were removed with 200 µL concentrated H_2O_2 (Suprapur®). Following repeated evaporation and dissolution, sample solutions were diluted with 4 mL MQ water and neutralized with 0.1 mL 1 mol L^{-1} HCl [*Reynolds et al.*, 2008]. Prior to isotopic analysis, all samples were chromatographically purified with 1 mL precleaned AG50W-X8 cation exchange resin (BioRad®, mesh 200–400) [after *Georg et al.*, 2006b; *de Souza et al.*, 2012b]. The silicon isotope ratios were analyzed on a NuPlasma high-resolution multicollector inductively

Table 1. The $\delta^{30}Si$ of *E. rex* Frustules (>154 μm Fraction) for Cores WPD-03 and WPD-12

Core	Interval (cm)	Age (kyr)	$\delta^{30}Si$ (‰)	$2\sigma_{sd}$ (‰)
WPD-03	0–10	19.53	−0.95	0.21
	60–65	21.55	−1.18	0.23
	100–105	22.95	−1.03	0.19
	140–145	24.35	−0.98	0.14
	180–185	25.75	−1.05	0.24
	212–214	26.82	−1.12	0.20
	228–230	27.38	−1.23	0.15
	252–254	28.23	−1.10	0.18
	284–286	29.35	−1.14	0.28
	292–294	29.63	−1.17	0.44
	300–302	29.91	−0.97	0.41
	312–314	30.33	−1.00	0.20
	316–318	30.47	−1.15	0.25
	324–326	30.75	−0.83	0.20
WPD-12	6–8		−0.89	0.22
	22–24		−0.87	0.15
	54–56		−1.05	0.26
	88–90		−1.03	0.27
	96–98		−1.02	0.21

coupled plasma–mass spectrometer by applying a standard-sample bracketing method [*Albarède et al*., 2004] at GEOMAR in Kiel, Germany, with selected replicate samples analyzed at the University of California, Santa Barbara (UCSB). All solutions were diluted to 0.6 ppm (measured colourimetrically using a photospectrometer per methods of *Grasshoff et al*. [1999]) and introduced via a CetacAridus II desolvating nebulizer system equipped with a perfluoroalkoxy nebulizer, yielding a 70–80 μL min^{-1} uptake rate. For methods used at UCSB to analyze sample duplicates, see *Brzezinski et al*. [2006].

The silicon isotopic compositions are reported in δ notation using the reference standard National Bureau of Standards (NBS) 28 in parts per thousand ($\delta^{30}Si = ((R_{sample}/R_{standard}) - 1) \times 1000$), where R_{sample} is the $^{30}Si/^{28}Si$ ratio of the sample and $R_{standard}$ is the $^{30}Si/^{28}Si$ ratio of the standard. For each sample, measurements were repeated at least on three different days and at least 4–5 times per session, which generally resulted in internal reproducibility between 0.14‰ and 0.28‰ ($2\sigma_{sd}$), with two samples having higher $2\sigma_{sd}$ of 0.41‰ and 0.44‰, respectively (Table 1). Repeated measurements of the reference materials NBS28, Institute for Reference Materials and Measurement 018, and Big Batch gave average $\delta^{30}Si$ values of 0.00 ± 0.26‰ ($2\sigma_{sd}$), −1.42 ± 0.27‰ ($2\sigma_{sd}$), and −10.64 ± 0.23‰ ($2\sigma_{sd}$), respectively. These values are in good agreement with values obtained by other laboratories [*Reynolds et al*., 2007; *Hendry et al*., 2011]. Replicate measurements of an in-house diatom matrix standard over longer periods of time ($n = 30$ sessions within 1 year) gave an external reproducibility of ±0.25‰ ($2\sigma_{sd}$).

3. Results

In core WPD-03, $\delta^{30}Si_{E.\ rex}$ ranges from −1.23‰ to −0.83‰ with an average of approximately −1.06‰ (Table 1 and Figure 4a). In core WPD-12, $\delta^{30}Si_{E.\ rex}$ varies from −1.05‰ to −0.87‰ with an average of approximately −0.97‰ (Table 1 and Figure 4e). The ranges of variation in $\delta^{30}Si_{E.\ rex}$ are thus 0.40‰ and 0.18‰ in the WPD-03 and WPD-12 cores, respectively. These ranges are rather small, just within the long-term external reproducibility (±0.25‰, $2\sigma_{sd}$) of the $\delta^{30}Si$ measurements (Figures 4a and 4e). They indicate that $\delta^{30}Si_{E.\ rex}$ is relatively invariant and does not exhibit pronounced changes within or between the two cores.

The $\delta^{30}Si_{E.\ rex}$ results of the present study (average −1.04 ± 0.22‰; $2\sigma_{sd}$, $n = 19$) are the most negative silicon isotopic compositions so far reported for diatoms and diatomaceous sediments of any age (Figure 5). To verify that these unusual diatom $\delta^{30}Si$ values are free from analytical bias, three *E. rex* sample duplicates (>154 μm fraction) from core WPD-03 were sent to UCSB for silicon isotopic analysis. Table 2 compares the results for the two laboratories, which are indistinguishable from each other within the reported error for each sample. These observations suggest that our $\delta^{30}Si_{E.\ rex}$ results can be regarded as a real environmental signal.

Unlike $\delta^{30}Si_{E.\ rex}$, the productivity proxies $\delta^{13}C_{E.\ rex}$ and $\delta^{13}C_{org}$ (Figure 4b), opal concentration (Figure 4c), and Ba/Ti [*Xiong et al*., 2012b] show a two-step pattern of change within LDM-03. These proxies increased through time during deposition of the PC, DC, and lower LDM-03, followed by stabilization at relatively high levels during deposition of the middle to upper LDM-03 [*Xiong et al*., 2012b, 2013a]. Illite content and illite/smectite ratios show a pronounced peak during DC deposition, followed by lower and relatively invariant values during deposition of the LDM-03 (Figure 4d). Core WPD-12 and the correlative portion of core WPD-03 show nearly identical lithofacies patterns as well as downcore geochemical trends (Figures 4e–4h).

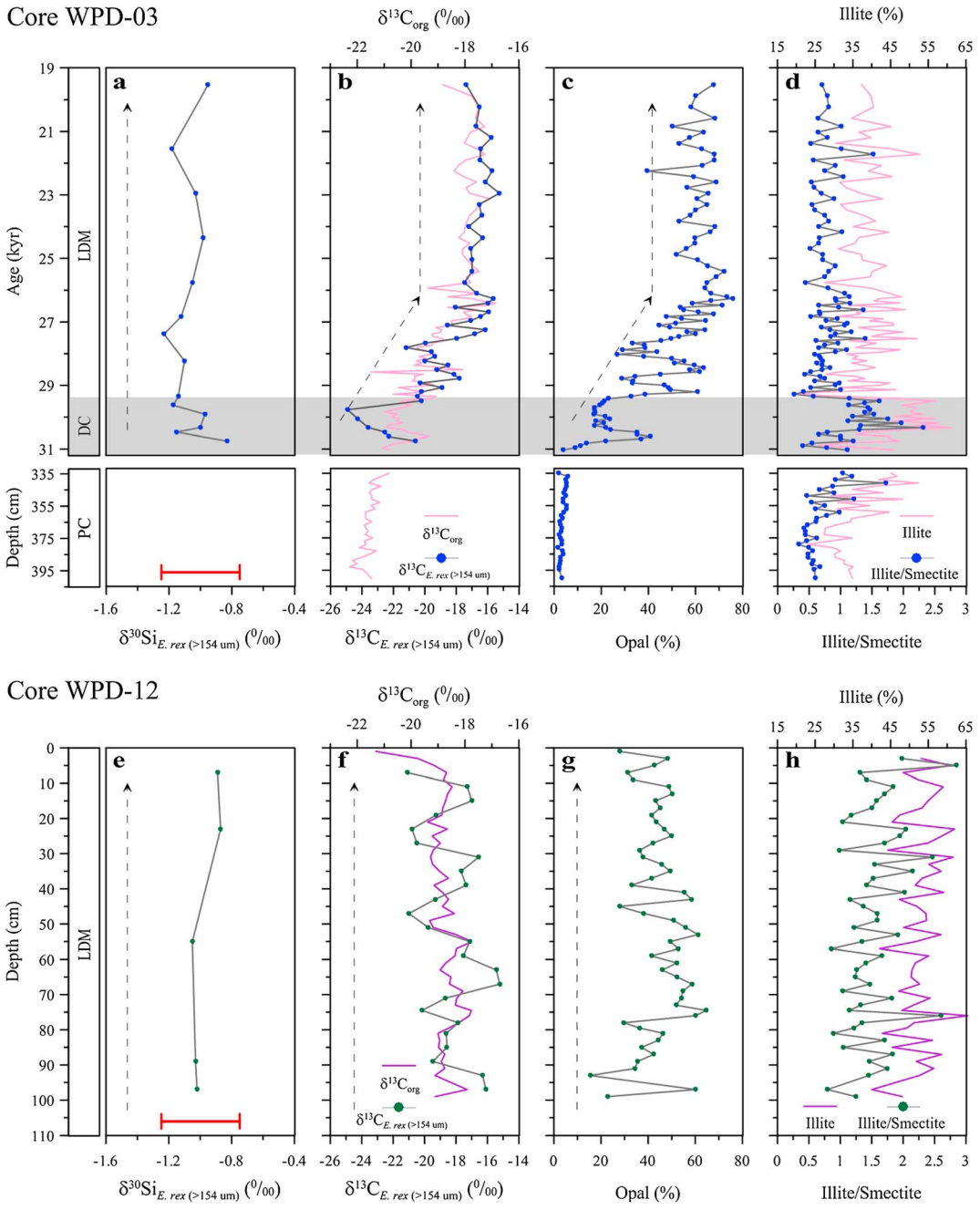

Figure 4. Age-depth profiles for $\delta^{30}Si_{E.\ rex}$, $\delta^{13}C_{E.\ rex}$, and $\delta^{13}C_{org}$; opal content; and illite content and illite/smectite ratios in cores (a–d) WPD-03 and (e–h) WPD-12. The error bars in Figures 4a and 4e show the long-term external reproducibility (±0.25‰, $2\sigma_{sd}$) of the $\delta^{30}Si$ measurements. The arrows in Figures 4a–4c and 4e–4g show general stratigraphic trends. Data in Figures 4a, 4e, 4f, and 4h are original to this study; data in Figures 4b–4d and 4g are from *Xiong et al.* [2012a, 2012b, 2013a]. LDM: laminated *E. rex* diatom mats, DC: diatomaceous clay, and PC: pelagic clay.

4. Discussion

4.1. Comparison With $\delta^{30}Si$ of Modern and Ancient Diatoms

The $\delta^{30}Si_{E.\ rex}$ results of the present study (average -1.04 ± 0.22‰; $2\sigma_{sd}$, $n = 19$) are exceptionally low compared to earlier studies of biogenic silica (BSi) and diatoms in the oceanic water column and sediment, which have yielded $\delta^{30}Si$ that is mostly >0‰ (Figure 5). The few instances of modern $\delta^{30}Si$ of <0‰ have been attributed to contributions of BSi from sponge spicules or radiolarians [*Cardinal et al.*, 2007; *Cao et al.*, 2012;

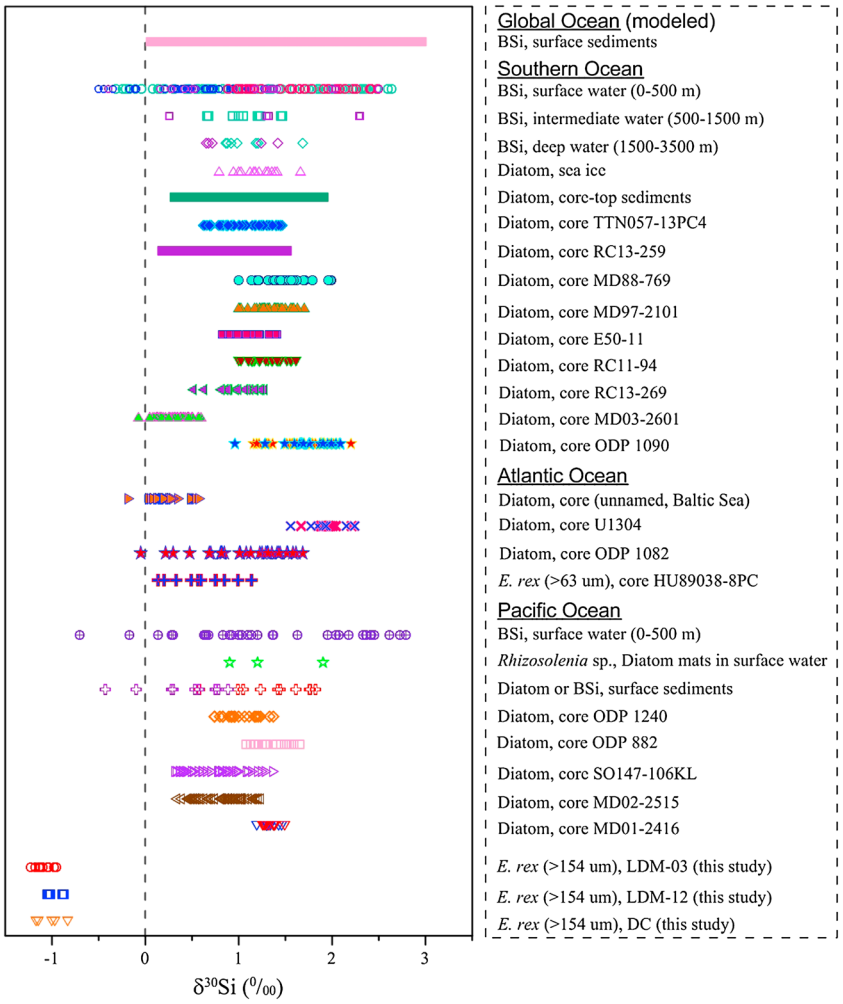

Figure 5. Comparison of $\delta^{30}Si_{E.\ rex}$ in cores WPD-03 and WPD-12 with published $\delta^{30}Si$ of diatoms or BSi in the oceanic water column and sediment. Data sources: global-ocean surface sediments [*Wischmeyer et al.*, 2003]; Southern Ocean surface waters (open circles), intermediate waters (open squares), and deep waters (open diamonds) (green [*Varela et al.*, 2004], blue [*Cardinal et al.*, 2007], red [*Fripiat et al.*, 2011b], and purple [*Fripiat et al.*, 2012]); Southern Ocean sea ice [*Fripiat et al.*, 2007], core-top sediments [*Egan et al.*, 2012], core TTN057-13PC4 [*Horn et al.*, 2011], core RC13-259 [*Brzezinski et al.*, 2002], cores MD88-769 and MD97-2101 [*Beucher et al.*, 2007], cores E50-11, RC11-94, and RC13-269 [*De La Rocha et al.*, 1998], core MD03-2601 [*Panizzo et al.*, 2014], and core ODP 1090 (2–10 μm (red pentacles) and 10–20 μm (blue pentacles) diatoms [*Egan et al.*, 2013]; Atlantic Ocean unnamed core (Baltic Sea) [*Sun et al.*, 2011], core U1304 [massive (blues crosses) and laminated (red crosses) diatom oozes [*Romero et al.*, 2011], core ODP 1082 [*Etourneau et al.*, 2012], and core HU89038-8PC [*Hendry et al.*, 2014]; and Pacific Ocean surface waters [*Cao et al.*, 2012], *Rhizosolenia* sp. [*De La Rocha et al.*, 2000], surface sediments (diatom (red open crosses) and BSi (purple open crosses) [*Ehlert et al.*, 2012], core ODP 1240 [*Pichevin et al.*, 2009], core ODP 882 [*Reynolds et al.*, 2008], core SO147-106KL [*Ehlert et al.*, 2013], core MD02-2515 [*Pichevin et al.*, 2012], and core MD01-2416 (10–20 μm (red triangles) and >63 μm (blue triangles) diatoms [*Maier et al.*, 2013]. Note that the $\delta^{29}Si$ data from *Cardinal et al.* [2007] and *Fripiat et al.* [2007] in Figures 5–7 were converted to $\delta^{30}Si$ by multiplication by a factor of 1.96 assuming mass-dependent fractionation under kinetic processes [*Reynolds et al.*, 2007].

Table 2. Interlaboratory Comparison of $\delta^{30}Si$ for Three *E. rex* Samples (>154 μm Fraction)

				UCSB			
		GEOMAR (November 2013)		First Analysis (October 2013)		Second Analysis (December 2013)	
Core	Interval (cm)	$\delta^{30}Si$ (‰)	$2\sigma_{sd}$ (‰)	$\delta^{30}Si$ (‰)	$2\sigma_{sd}$ (‰)	$\delta^{30}Si$ (‰)	$2\sigma_{sd}$ (‰)
WPD-03	100–105	−1.03	0.19	−1.00	0.05	−0.93	0.08
	180–185	−1.05	0.24	−1.08	0.05	−0.98	0.19
	252–254	−1.10	0.18	−1.11	0.10	− 1.07	0.05

Egan et al., 2012; *Ehlert et al*., 2012], whose δ^{30}Si is on average lighter than that of diatoms [*Ding et al*., 1996; *Wu et al*., 1997; *De La Rocha*, 2003; *Ellwood et al*., 2010; *Hendry and Robinson*, 2012]. Two earlier studies suggested that modern and ancient giant diatoms also generally yield δ^{30}Si of >0‰ (Figure 5): (1) the δ^{30}Si of *Rhizosolenia* sp. from diatom mats in surface waters of the central North Pacific is +0.9‰ to +1.9‰ [*De La Rocha et al*., 2000] and (2) the δ^{30}Si of the >63 μm *E. rex* fraction extracted from a sediment core in the North Atlantic ranged from +0.2‰ to +1.14‰ [*Hendry et al*., 2014]. Differences in δ^{30}Si between modern and ancient diatom species and *E. rex* from the LGM (this study) probably reflect different DSi sources prevailing during their blooms (see section 4.4.1).

4.2. Potential DSi Sources to the Eastern Philippine Sea

There are multiple potential DSi sources to the EPS, which we will consider in the context of the global silicon cycle. DSi is delivered to the global ocean via four main pathways, i.e., the riverine, eolian, hydrothermal, and submarine basalt weathering fluxes [*Tréguer et al*., 1995]. As an open pelagic deep sea with a water depth of ~5000 m (Figure 1), the EPS does not receive DSi input directly from rivers. Furthermore, inputs of DSi from hydrothermal and basalt weathering sources in the EPS are small and strongly diluted before transport to the surface mixed layer [*Harrison*, 2000]. Thus, these three fluxes are unlikely to have been the proximate cause of giant diatom blooms in the EPS during the LGM. The only significant external flux of silicon to the surface layer of the EPS is the DSi derived from eolian dust (DSi_{eolian}). The principal alternative to DSi_{eolian} as a nutrient source for giant diatom blooms is upwelling of DSi ($DSi_{upwelled}$) from subsurface (~100–500 m) and/or intermediate (~500–1500 m) depths to the surface layer of the EPS, a process that has been shown to play an important role in diatom blooms in other oceanic regions [*Tréguer et al*., 1995; *Ragueneau et al*., 2000; *Tréguer and De La Rocha*, 2013].

Many diatoms, especially spring-bloom species, utilize subsurface- and intermediate-water DSi that is upwelled or advected into the surface mixed layer. In the tropical western Pacific, subsurface- and intermediate-depth waters derive from mixing of Subantarctic Mode Water (SAMW), Antarctic Intermediate Water (AAIW), and North Pacific Intermediate Water (NPIW) [*Toggweiler et al*., 1991; *Qu et al*., 1999; *Qu and Lindstrom*, 2004; *Kawabe and Fujio*, 2010; see review in *Bostock et al*., 2010] (Figure 2d). Although some investigators have argued that Equatorial Pacific Intermediate Water (EqPIW) is a separate water mass [*Bingham and Lukas*, 1995; *Firing et al*., 1998; *Bostock et al*., 2010], EqPIW probably forms from mixing AAIW with a smaller component of upwelled Pacific Deep Water [*Bostock et al*., 2010], so we will regard it as part of AAIW in the following discussion.

Northward advection of SAMW and AAIW controls the nutrient distribution and biological productivity of surface waters of the tropical Pacific [*Sarmiento et al*., 2004; *Marinov et al*., 2006]. At present (i.e., in interglacial times), SAMW and AAIW are characterized by low DSi and high nitrate concentrations as a result of greater uptake of DSi relative to nitrate by diatoms in the Southern Ocean [*Sarmiento et al*., 2004, 2007]. In contrast, high DSi and low nitrate concentrations prevailed in the SAMW and AAIW during glacial periods due to enhanced utilization of nitrate by Southern Ocean diatoms in response to elevated eolian iron fluxes [*Brzezinski et al*., 2002; *Beucher et al*., 2007]. Northward transport of unutilized DSi by SAMW and AAIW then resulted in enhanced tropical-ocean diatom productivity [*Brzezinski et al*., 2002; *Matsumoto et al*., 2002]. This hypothesis is supported by opal records from the equatorial Atlantic and eastern tropical Pacific, which show higher BSi mass accumulation rates (MAR) during glacials relative to interglacials [*Bradtmiller et al*., 2007; *Arellano-Torres et al*., 2011]. However, some authors have questioned this scenario based on the observation that opal fluxes peaked during the last deglaciation and marine isotope stage 3 rather than during the LGM [e.g., *Kienast et al*., 2006; *Dubois et al*., 2010]. Recently, by emphasizing the role of Southern Ocean and tropical-ocean ventilation in delivery of DSi during the deglaciation, the former "silicic acid leakage hypothesis" has been revised to the "silicic acid ventilation hypothesis" [*Crosta et al*., 2007; *Hendry and Brzezinski*, 2014]. However, enhanced DSi supply from the Southern Ocean during the LGM has not been demonstrated for the western tropical Pacific region to date.

Southward advection of NPIW may be another vector for resupply of DSi to the EPS. In contrast to SAMW and AAIW, NPIW is rich in both DSi (Figure 2c) and nitrate, and it is known to strongly influence productivity in the northern and equatorial Pacific [*Tsunogai*, 2002; *Sarmiento et al*., 2004]. However, paleoceanographic evidence of a link between NPIW ventilation and glacial diatom production in the western tropical Pacific is lacking. In addition, North Pacific Deep Water (NPDW), which is characterized by maximum silicate

concentrations of $>144\,\mu mol\,kg^{-1}$, also reaches the EPS from the northeastern Pacific via westward flow from the Hawaiian Islands [*Siedler et al.*, 2004] (Figure 1). Considering its water depth (2000–3500 m), NPDW can rise to intermediate depths but cannot directly feed the thermocline of the EPS. In summary, lateral advection of oceanic water masses rich in DSi represents a potential source of nutrient silicon to surface waters of the EPS during the LGM, although an indirect one that would have been attenuated by mixing and dilution effects.

An important source of silicon to surface waters of the EPS is Asian dust. Asian dust is transported over wide areas of the Pacific Ocean (see review in *Rea* [2007]) and is even carried as far eastward as North America [*McKendry et al.*, 2001], northern Europe [*Bory et al.*, 2003], and in a full circuit around the globe [*Uno et al.*, 2009]. Numerous observations and climate models have demonstrated that Asian dust is delivered to the tropical western Pacific Ocean by the Northern Hemisphere westerlies and the East Asian winter monsoon (EAWM) [*Nilson and Lehmkuhl*, 2001; *Shao et al.*, 2011; *Muhs*, 2013]. Radiogenic Sr-Nd isotopic data from surface and subsurface sediments suggest that Asian dust contributes ~10–50% of the detrital fraction of the surface sediments in the western Philippine Sea [*Jiang et al.*, 2013]. In the Parece Vela Basin of the EPS, the proportion of Asian dust in the detrital fraction is higher, ranging from 50% to 70%, reflecting the influence of an average Asian dust MAR of ~0.45 $g\,m^{-2}\,yr^{-1}$ (F. Jiang, unpublished data). Furthermore, the flux of Asian dust to the Philippine Sea may have been even greater during late Pleistocene glacial periods, as inferred from clay-mineral and major-element data [*Wan et al.*, 2012; *Xu et al.*, 2012, 2013]. In cores WPD-03 and WPD-12, the presence of substantial quantities of illite in the DC and LDM are indicative of continuous Asian eolian inputs during the LGM [*Xiong et al.*, 2010, 2013a] (Figures 4d and 4h; see section 4.4.1).

The flux of eolian dust to the ocean influences marine biogeochemistry and global climate by regulating the supply of iron and silicon, both of which can be productivity-limiting nutrients [*Maher et al.*, 2010]. According to a recent oceanic silicon budget, ~5% of seawater silicon is sourced by eolian processes [*Tréguer and De La Rocha*, 2013]. Given that silicon in the global ocean is dominated by DSi rather than BSi, the contribution of eolian dust to seawater DSi is thus ~5% or slightly more. Although this contribution is relatively small at a global scale, eolian dust may be the primary external source of DSi in the open pelagic ocean (e.g., the EPS) where rivers have little influence [*Duce et al.*, 1991]. Enhanced eolian silicon inputs during glacial times are hypothesized to have promoted diatom blooms, resulting in increased primary and export productivity as well as organic carbon burial [*Harrison*, 2000; *Nozaki and Yamamoto*, 2001]. A direct link between the Asian dust flux and diatom productivity in the North Pacific region has been confirmed by both modern observations and paleoceanographic studies [e.g., *Kawahata et al.*, 2000; *Yuan and Zhang*, 2006]. This relationship has also been documented for the oligotrophic subtropical Shikoku Basin (just north of the EPS) on the basis of time series sediment-trap studies [*Li et al.*, 2004]. Analysis of aerosols from the North Pacific has shown that the mineralogic composition of Asian dust is dominated by aluminosilicates and quartz [*Gao et al.*, 2007]. Although only ~5% of this eolian silicon is directly dissolved when the particles enter seawater [*Duce et al.*, 1991], additional DSi can be leached from settling dust particles in seawater, providing nutrient silicon for diatom blooms [*Yuan and Zhang*, 2006]. The leaching process is thought to be similar to submarine weathering of silicate minerals, in which reactions with dissolved CO_2 yield DSi [*Scholz et al.*, 2013].

4.3. Modeling DSi Sources to the Eastern Philippine Sea

4.3.1. Biogenic Silicon Isotope Fractionation ($^{30}\varepsilon$)

Isotopic fractionation during the incorporation of DSi into BSi is expressed as $^{30}\varepsilon$, i.e., the fractionation factor representing the instantaneous (i.e., nonaccumulated) enrichment or depletion of ^{30}Si in BSi compared to the parent DSi. The fractionation factor $^{30}\varepsilon$ can be assessed empirically based on $\Delta^{30}Si$, which is the difference in $\delta^{30}Si$ between sedimentary BSi and aqueous DSi (i.e., $\Delta^{30}Si = \delta^{30}Si_{diatom} - \delta^{30}Si_{DSi}$) [*Cardinal et al.*, 2007; *Fripiat et al.*, 2012]. The silicon isotopic fractionation during BSi formation by diatoms can be described in terms of either a Rayleigh (closed-system) model or a steady state (open-system) model [*Fry*, 2006]. In the open-system model, $\Delta^{30}Si$ is constant and equal to $^{30}\varepsilon$ due to the simple overall isotope dynamics. In the closed-system model, $\Delta^{30}Si$ increases relative to $^{30}\varepsilon$ during DSi consumption because $\delta^{30}Si_{diatom}$ reflects the accumulated rather than the instantaneous $\delta^{30}Si$ composition of BSi. However, at a low fraction of DSi consumed, $\Delta^{30}Si$ is effectively equal (e.g., within measurement error) to $^{30}\varepsilon$ in the closed system (i.e., $\Delta^{30}Si \approx {}^{30}\varepsilon$) [*Cardinal et al.*, 2007; *Demarest et al.*, 2009; *Cao et al.*, 2012].

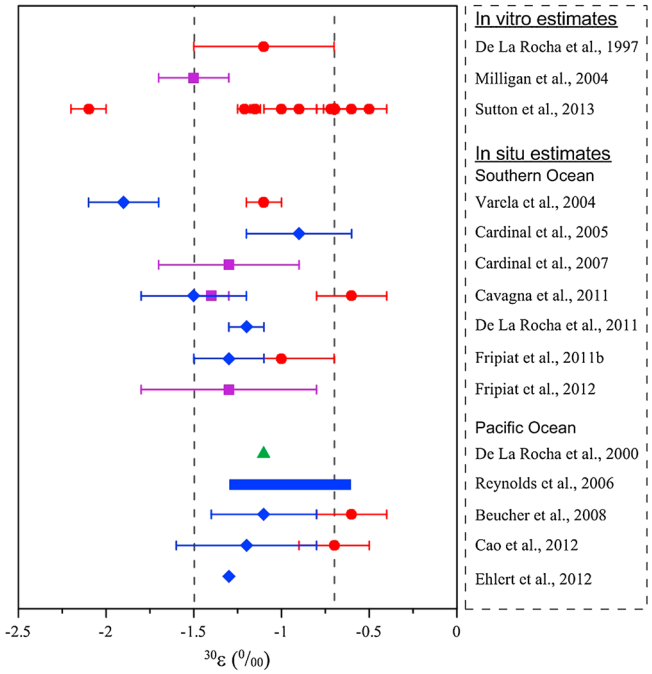

Figure 6. Estimates of the silicon isotopic fractionation factor ($^{30}\varepsilon$) during silicic acid assimilation by marine diatoms based on in vitro experiments and in situ observations. The red and blue symbols represent $^{30}\varepsilon$ estimates using the closed-system and open-system models, respectively. The purple symbols represent $^{30}\varepsilon$ estimates for which Δ^{30}Si was substituted, and the green symbol is an estimate based on linear regression of $\delta^{30}Si_{DSi}$ against ln[DSi]. The vertical dashed lines bracket the $^{30}\varepsilon$ range of *De La Rocha et al.* [1997].

Recent studies have mostly yielded a relatively narrow, consistent set of $^{30}\varepsilon$ values. Culture experiments under closed-system conditions yielded $^{30}\varepsilon$ estimates of -1.1 ± 0.4‰ [*De La Rocha et al.*, 1997] and -1.5 ± 0.2‰ [*Milligan et al.*, 2004], which are identical within the reported error. Similar values were obtained in field studies of Pacific and Southern Ocean diatoms, with $^{30}\varepsilon$ estimates generally in the range of -1.5‰ to -0.7‰ (Figure 6). Modeling of $^{30}\varepsilon$ for closed (-1.1 ± 0.1‰) and open systems (-1.9 ± 0.2‰) suggested that Antarctic Circumpolar Current surface waters are intermediate between these end-members [*Varela et al.*, 2004]. The limited variation among these estimates implies that $^{30}\varepsilon$ may be largely independent of species, temperature, growth rates, pH, salinity, and cell size [*De La Rocha et al.*, 1997; *Milligan et al.*, 2004; *Alleman et al.*, 2005; *Cardinal et al.*, 2007]. For this reason, we will assume that $^{30}\varepsilon$ averages -1.1‰ and that measured Δ^{30}Si values are equal to $^{30}\varepsilon$ for modeling purposes in this study.

We recognize that certain studies have documented significant variability in Δ^{30}Si or $^{30}\varepsilon$. For example, *Fripiat et al.* [2012] reported a latitudinal dependence of Δ^{30}Si, with variation from -0.3‰ at 45–50°S to -1.7‰ at lower and higher latitudes. In that study, smaller Δ^{30}Si values were associated with lower DSi concentrations, reflecting minimal fractionation at high degrees of DSi utilization as predicted by the closed-system model, and the larger values of Δ^{30}Si are thus probably closer to true $^{30}\varepsilon$. *Hendry et al.* [2014] documented substantial Δ^{30}Si variation in *E. rex*, from -0.46‰ to -1.4‰ (based on $\delta^{30}Si_{diatom}$ of +0.2‰ to +1.14‰ and an AAIW source δ^{30}Si of +1.6‰; Figure 5). They inferred that simple fractionation models cannot account for the observed $\delta^{30}Si_{diatom}$ values and that the large degree of variability is related to dynamic water mass mixing. A culture experiment by *Sutton et al.* [2013] yielded $^{30}\varepsilon$ estimates ranging from -0.54‰ to -2.09‰ for different diatom species, suggesting species-specific fractionation factors (Figure 6). However, other studies do not support this inference. For example, *Egan et al.* [2013] found that different diatom size fractions (and, thus, species assemblages) in Southern Ocean core-top samples yielded similar δ^{30}Si, suggesting minimal interspecific variation. In general, the observed variations in $^{30}\varepsilon$ estimates are likely to reflect uncertainties in initial conditions, difficulties in accurately determining DSi sources, complexities in water mass mixing dynamics, and limitations in existing fractionation models [*Reynolds et al.*, 2006; *Beucher et al.*, 2008; *Fripiat et al.*, 2011b, 2012; *Egan et al.*, 2012; *Ehlert et al.*, 2013].

4.3.2. Model Constraints on DSi Sources

We developed a binary mixing model to evaluate DSi sources for *E. rex* blooms in the EPS during the LGM (Figure 7a). In this model, the two end-members are upwelled silicon and eolian silicon (see section 4.2). The application of this model depends on differences in the silicon isotopic composition between subsurface/intermediate water masses and Asian dust (see section 4.4.1).

Subsurface and intermediate waters of the Pacific region show a limited range of positive δ^{30}Si values. Reported δ^{30}Si values are (1) AAIW = +1.25 to +1.8‰ [*Cardinal et al.*, 2005; *Fripiat*, 2010; *de Souza et al.*,

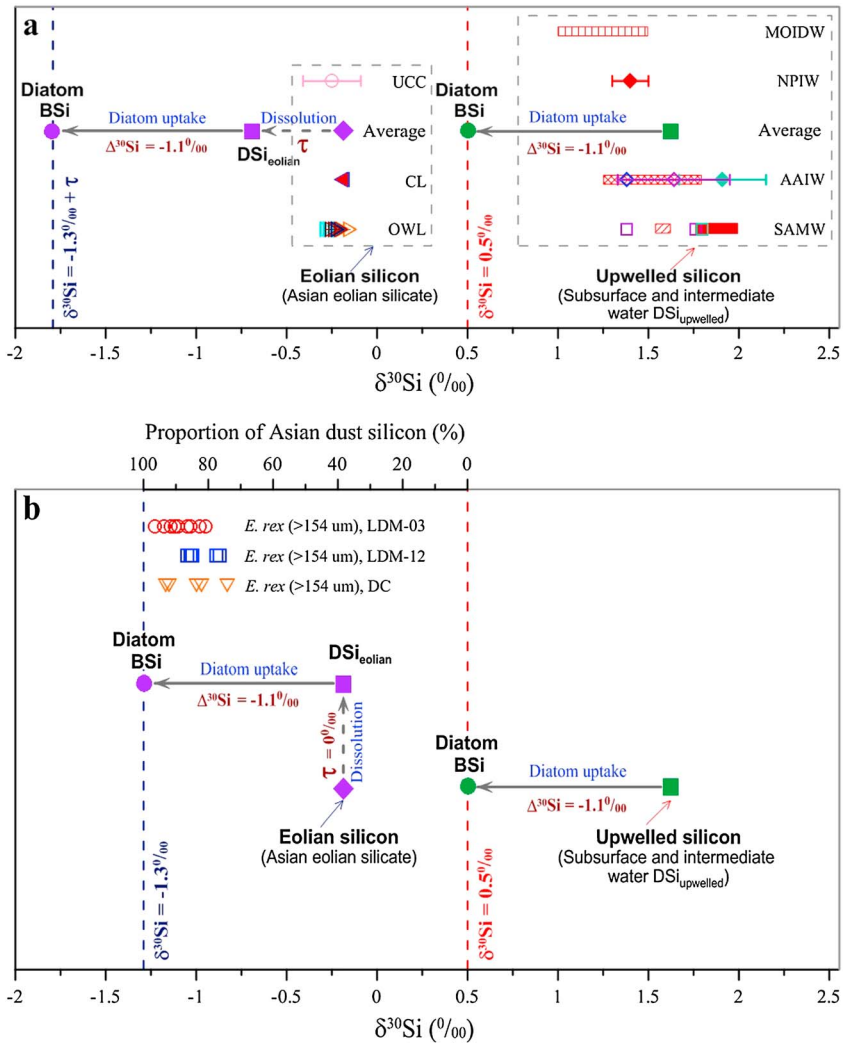

Figure 7. Binary mixing model for discrimination of sources of DSi utilized in *E. rex* blooms in the EPS during the LGM. (a) Construction of the binary mixing model, based on an upwelled silicon end-member with δ^{30}Si of +1.6‰, an eolian dust silicon end-member with δ^{30}Si of −0.2‰, a variable fractionation during silicate dissolution of τ (probably between −0.3‰ and 0‰), and biotic assimilatory fractionation of −1.1‰. (b) Calculation of proportion of DSi sourced from upwelled silicon versus eolian silicon, based on measured $\delta^{30}Si_{E.\ rex}$ in cores WPD-03 and WPD-12 (for assumed τ = 0‰). In Figure 7a, τ is shown as equal to −0.5‰, although the actual value of τ is unknown. In Figures 7a and 7b, the difference in silicon isotopic compositions between diatom BSi and DSi (Δ^{30}Si) of −1.1‰ represents an estimate of $^{30}\varepsilon$. UCC is upper continental crust, CL is Chinese loess, OWL is other worldwide loess, and MOIDW is modeled ocean intermediate and deep water; see Figure 1 for other abbreviations. The dashed vertical lines represent estimated end-member compositions for *E. rex* in the EPS during the LGM for DSi derived 100% from eolian dust (blue) or upwelled silicon (red). The purple diamonds and green squares represent estimated average values for eolian silicon and upwelled silicon, respectively. Data sources for δ^{30}Si: SAMW (red filled rectangle [*Cardinal et al.*, 2005; *Fripiat*, 2010], purple and green empty squares [*de Souza et al.*, 2012a], and red empty rectangle [*de Souza et al.*, 2012b]); AAIW (red empty rectangle [*Cardinal et al.*, 2005; *Fripiat*, 2010; *de Souza et al.*, 2012a, 2012b], blue empty diamond [*Reynolds*, 2009], and purple empty diamond and green filled diamond [*Fripiat et al.*, 2011a]); MOIDW [*Wischmeyer et al.*, 2003]; NPIW [*Reynolds et al.*, 2006]; and UCC, CL, and OWL [*Savage et al.*, 2013]. See sections 4.2 and 4.3 for further details.

2012a, 2012b], +1.38‰ [*Reynolds*, 2009], and +1.64 ± 0.31‰ and +1.91 ± 0.24‰ [*Fripiat et al.*, 2011a]; (2) SAMW = +1.75 to +2.0‰ [*Cardinal et al.*, 2005; *Fripiat*, 2010], +1.55 to +1.60‰ [*de Souza et al.*, 2012b], and +1.38‰, +1.76‰ and +1.8‰ [*de Souza et al.*, 2012a]; and (3) NPIW = +1.4 ± 0.1‰ [*Reynolds et al.*, 2006]. These values are consistent with simulations yielding estimated δ^{30}Si of +1.0‰ to +1.5‰ for intermediate and deep waters of the world ocean (MOIDW) [*Wischmeyer et al.*, 2003]. These results demonstrate that subsurface and intermediate water δ^{30}Si is >+1.0‰ throughout the modern global ocean. We adopt an

estimate of +1.6‰ as the average value for the $DSi_{upwelled}$ supporting diatom growth in EPS surface waters and +0.5‰ as the average $\delta^{30}Si$ of diatom silica generated from $DSi_{upwelled}$ (i.e., reflecting $^{30}\varepsilon = -1.1‰$; Figure 7a).

Although the $\delta^{30}Si$ of eolian dust from marine sediments is poorly known, that of continental eolian dust (e.g., loess) has been well studied. *Savage et al.* [2013] systematically analyzed Pleistocene loess samples from China, New Zealand, Germany, Hungary, and the U.S., thus characterizing typical silicon isotopic compositions of continental dust globally. The $\delta^{30}Si$ of loess shows minor variation among different regions, ranging from −0.28‰ to −0.15‰ (average $-0.22 \pm 0.07‰$ ($2\sigma_{sd}$)) [*Savage et al.*, 2013]. In particular, Chinese loess displays an average $\delta^{30}Si$ of $-0.19 \pm 0.22‰$ ($2\sigma_{sd}$) ($-0.20 \pm 0.08‰$ ($2\sigma_{sd}$) for repeat analyses) [*Savage et al.*, 2013]. The main sources of Asian dust are the eastern and central Asian deserts (e.g., the Taklamakan, Gobi/Badin Jaran, and Tengger) [*Nilson and Lehmkuhl*, 2001; *Shao et al.*, 2011; *Muhs*, 2013]. Assuming negligible silicon isotopic fractionation of Asian dust during transport to the tropical West Pacific, the eolian dust delivered to marine areas should have a Si-isotopic composition similar to that of Chinese loess. Thus, we adopt −0.2‰ as an estimate of the average $\delta^{30}Si$ of Asian dust deposited in the EPS (Figure 7a).

The silicon isotopic composition of silicate materials can undergo changes during their dissolution. Silicate dissolution preferentially releases ^{28}Si [*Ziegler et al.*, 2005; *Opfergelt and Delmelle*, 2012; *Cornelis et al.*, 2014], suggesting that the DSi generated from the dissolution of eolian dust may have a lower $\delta^{30}Si$ than the parent material. However, the silicon isotope fractionation associated with release of DSi from silicates has not been well constrained and may depend on the mineral composition of the dust. Here we accommodate this uncertainty by assigning an unknown quantity τ (with a negative value) to represent the $\delta^{30}Si$ difference between Asian eolian silicon and the DSi_{eolian} released to seawater. Thus, the $\delta^{30}Si$ of DSi_{eolian} is $-0.2‰ + \tau$, and the $\delta^{30}Si$ of diatom silica made from such DSi_{eolian} is $-1.3‰ + \tau$ (i.e., accounting for $^{30}\varepsilon = -1.1‰$; Figure 7a).

One point of uncertainty is whether subsurface- and intermediate-water $\delta^{30}Si$ was the same in the late Pleistocene ocean as in the modern. We cannot evaluate $\delta^{30}Si$ differences between the LGM and the Holocene, but *Maslin and Swann* [2006] argued that seawater shows minimal variability in $\delta^{30}Si$ at glacial-interglacial time scales. A second point of uncertainty is silicon isotopic fractionation associated with dissolution during the export and burial of diatom frustules. *Demarest et al.* [2009] reported that BSi dissolution preferentially releases light ^{28}Si with a fractionation factor of −0.55‰. Thus, the $\delta^{30}Si$ of preserved BSi may be shifted toward more positive values than that of initial BSi. However, given the current analytical uncertainty of ~0.1‰ for $\delta^{30}Si$ measurements [*Reynolds et al.*, 2007], the $\Delta^{30}Si$ between initial and preserved BSi will be detectable only when dissolution amounts to >20% of total BSi [*Demarest et al.*, 2009]. This is roughly consistent with the estimate of *De La Rocha et al.* [1998] that diatoms can retain their original $\delta^{30}Si$ signature even after dissolution of 26% of BSi. Several investigations of core-top [*Egan et al.*, 2012], sediment trap [*Varela et al.*, 2004], and water column samples [*Cardinal et al.*, 2007; *Fripiat et al.*, 2012], as well as dissolution experiments on diatoms from cores [*Wetzel et al.*, 2014], confirm that dissolution and early diagenesis have little to no effect on $\delta^{30}Si$ in natural environments.

4.4. Comparative Data-Model Evaluation of DSi Sources

4.4.1. DSi Sources for *E. rex* Blooms During the LGM

Application of our binary mixing model shows that most samples from cores WPD-03 and WPD-12 yield $\delta^{30}Si_{E.\ rex}$ close to the eolian silicon end-member (Figure 7b). This observation strongly suggests that *E. rex* in the EPS dominantly utilized DSi_{eolian} rather than $DSi_{upwelled}$ from subsurface and intermediate waters during the LGM. Furthermore, one can calculate the proportion of silicon from each source based on measured $\delta^{30}Si_{E.\ rex}$ values. Exact proportions depend on the value chosen for τ, although reasonable variation in τ results in only limited uncertainties in calculated values. Assuming that $\tau = 0‰$, measured $\delta^{30}Si$ values of −1.23‰ to −0.83‰ (average −1.04‰) for *E. rex* in cores WPD-03 and WPD-12 correspond to 4–26% (average 14%) of diatom silica being derived from $DSi_{upwelled}$ and 74–96% (average 86%) being derived from DSi_{eolian} (Figure 7b). If $\tau = -0.3‰$, these proportions shift to 18–37% (average 27%) from $DSi_{upwelled}$ and 63–82% (average 73%) from DSi_{eolian}; if τ is positive (which is unlikely), then the proportion of DSi_{eolian} would be >74–96% (average >86%). Allowing $^{30}\varepsilon$ to vary has only a limited effect on model output. For example, if the silicon utilized by *E. rex* is 50% DSi_{eolian} and 50% $DSi_{upwelled}$, then $^{30}\varepsilon$ would be

−1.8‰ (assuming $\tau = 0‰$). As $DSi_{upwelled}$ becomes larger than 50%, $^{30}\varepsilon$ will rapidly exceed the upper end of reported $^{30}\varepsilon$ values obtained from culture experiments (i.e., −2.09‰ [*Sutton et al*., 2013]). These observations suggest that our model results (i.e., *E. rex* utilization of $DSi_{eolian} > DSi_{upwelled}$) are robust within the range of reported $^{30}\varepsilon$ values. Our $\delta^{30}Si_{E.\ rex}$ data thus clearly imply that DSi for *E.rex* blooms was derived mainly from Asian dust with smaller contributions from the Southern Ocean or North Pacific Ocean through lateral advection of SAMW, AAIW, or NPIW.

Evidence from clay minerals also supports the dominant usage of DSi_{eolian} for *E. rex* blooms in the EPS during the LGM. In the Philippine Sea, the two dominant clay minerals are illite and smectite, the former being sourced mainly from the Asian dust flux and the latter by weathering of volcanic materials on Luzon island or at the seafloor [*Xiong et al*., 2010; *Wan et al*., 2012; *Xu et al*., 2012]. High illite content and/or illite/smectite ratios represent a relative increase in wind shear and eolian dust inputs to the Philippine Sea [*Xiong et al*., 2010; *Wan et al*., 2012; *Xu et al*., 2012]. In cores WPD-03 and WPD-12, significant quantities of illite are present throughout the DC and LDM, indicating a substantial eolian dust supply (Figures 4d and 4h). Comparing the rare Earth elemental characteristics of EPS sediments with their potential sources, *Xu et al*. [2008] inferred that siliceous material of nonbiogenic origin (Figure 3c) was sourced primarily from alteration of seafloor basalts and secondarily from the eolian dust flux. Therefore, we assume that illite/smectite ratios reflect the relative contributions of Asian dust versus products of altered seafloor basalts.

The concentration of siliceous material of nonbiogenic origin can be roughly estimated by subtracting the opal concentration from the bulk sediment, due to the negligible presence of calcium carbonate and organic matter and only minor accumulation of authigenic phases [*Xiong et al*., 2012a, 2012b]. The Asian dust flux (F_{eolian}) can be calculated based on average opal, illite, and smectite concentrations (C_{opal}, C_{illite}, and $C_{smectite}$), linear sedimentation rate (LSR) (R), and dry bulk sediment density (D):

$$\begin{aligned} F_{eolian} &= (1 - C_{opal}) \times C_{illite} / (C_{illite} + C_{smectite}) \times R \times D \\ &= (1 - 47.5\%) \times 40.6\% \,/\, (40.6\% + 48.7\%) \times 27.4\ \text{cm kyr}^{-1} \times 2.42\ \text{g cm}^{-3} \times 10 \\ &= 158.3\ \text{g m}^{-2}\text{yr}^{-1} \end{aligned} \quad (1)$$

where 47.5%, 40.6%, 48.7%, 27.4 cm kyr^{-1}, and 2.42 g cm^{-3} are the average opal, illite, and smectite concentrations; LSR; and sediment density, respectively, during deposition of DC and LDM-03 [*Xiong et al*., 2012b, 2013a]. The estimated Asian dust flux in the EPS was 1–3 orders of magnitude greater than the general dust flux in the tropical Pacific during the LGM, which was about 0.1–10 g m^{-2} yr^{-1}, as determined from paleoceanographic records and model simulations [*Kohfeld and Harrison*, 2001; *Maher et al*., 2010]. Thus, we infer that a strong and relatively steady input of eolian dust from Asian sources during the LGM provided large quantities of nutrient silicon (and possibly iron also) for *E. rex* blooms in the EPS.

In order to test the validity of F_{eolian} (equation (1)), we make a simple mass balance comparison with the BSi burial flux (BF_{BSi}) in the EPS during the LGM. The BF_{BSi} during DC and LDM-03 can be calculated as follows:

$$\begin{aligned} BF_{BSi} &= 47.5\% \times (28.09 \,/\, 67.30) \times 27.4\ \text{cm kyr}^{-1} \times 2.42\ \text{g cm}^{-3} \times 10 \\ &= 131.5\ \text{g m}^{-2}\text{yr}^{-1} \end{aligned} \quad (2)$$

where 47.5%, 27.4 cm kyr^{-1}, 2.42 g cm^{-3}, 67.30, and 28.09 are the average opal concentration, LSR, sediment density, and the molar weights of opal ($SiO_2 \cdot 0.4\ H_2O$) and Si, respectively. This value of BF_{BSi} is close to that of F_{eolian} (158.3 g m^{-2} yr^{-1}) in the EPS during the LGM, satisfying the mass balance. Thus, we infer that Asian dust could have provided sufficient silicon for *E. rex* blooms during the LGM.

An interesting question is why *E. rex* did not bloom during DC deposition if there was strong eolian input at that time. In the WPD-03 core, the illite content and illite/smectite ratios rise substantially within the DC interval, with an average value roughly twice as high as those for the PC or LDM intervals (Figure 4d). These characteristics suggest such a rapid increase in the EAWM during DC deposition that it triggered strong wind-driven upwelling [*Xiong et al*., 2010, 2013a] and that upwelling then inhibited blooms of giant diatoms such as *E. rex* owing to their requirement for water mass stratification [*Gingele and Schmieder*, 2001; *De Deckker and Gingele*, 2002; *Kemp and Villareal*, 2013]. Wind-driven upwelling may have stimulated modest levels of small spring-bloom diatom productivity during DC deposition, as evidenced by an opal peak (Figure 4c), a maximum in small diatom abundance [*Zhai et al*., 2012], and high illite/smectite ratios (Figure 4d).

4.4.2. Degree of DSi Utilization for *E. rex* Blooms During the LGM

The degree of utilization of DSi in EPS surface waters during the LGM can be estimated from $\delta^{30}Si_{E.\ rex}$ variation in the WPD-03 and WPD-12 study cores. Before performing these calculations, it is necessary to consider whether other processes (e.g., diagenetic alteration, $\delta^{30}Si$ variability of the surface DSi reservoir, and DSi availability) could have influenced $\delta^{30}Si_{E.\ rex}$ [*De La Rocha et al*., 1998; *Reynolds et al*., 2008; *Romero et al*., 2011; *Pichevin et al*., 2012]. Little or no dissolution of BSi in the sediment is likely to have occurred given the high average LSR of WPD-03 (27.4 cm kyr^{-1} [*Xiong et al*., 2013a]), the intrinsically dense meshwork of *E. rex* LDMs [*Kemp and Baldauf*, 1993; *Bodén and Backman*, 1996], and SEM evidence for excellent preservation of *E. rex* frustules (Figure 3). Considering the dominant eolian source of DSi (see section 4.4.1) and stratified conditions of the EPS [*Gingele and Schmieder*, 2001; *De Deckker and Gingele*, 2002; *Kemp and Villareal*, 2013], the $\delta^{30}Si$ of the DSi source for *E. rex* blooms may have been nearly constant during the LGM. Although global seawater $\delta^{30}Si$ may change due to variations in the flux or $\delta^{30}Si$ of continental DSi inputs, this effect will be pronounced only at time scales longer than the residence time of DSi in seawater (~10 kyr [*De La Rocha and Bickle*, 2005; *Georg et al*., 2006a, 2009; *Tréguer and De La Rocha*, 2013]). The $\delta^{30}Si$ of DSi of EPS surface waters is thus unlikely to have changed appreciably during the 11.5 kyr interval of deposition of the DC and LDM in core WPD-03.

After excluding other processes that might have potentially influenced $\delta^{30}Si_{E.\ rex}$, we can interpret $\delta^{30}Si_{E.\ rex}$ as a function of degree of DSi utilization in EPS surface waters. The nearly uniform $\delta^{30}Si_{E.\ rex}$ values in the DC and LDM of both study cores imply a relatively constant degree of DSi utilization by *E. rex*. One possibility is that *E. rex* completely utilized available DSi in the EPS surface layer. In this case, observed $\delta^{30}Si_{E.\ rex}$ values should approach the silicon isotopic composition of source DSi, which was estimated at −0.2‰ for DSi_{eolian} assuming $\tau = 0$‰ (see section 4.4.1). However, this is clearly not the case (Figure 7b), so it is unlikely that *E. rex* exhausted the DSi of EPS surface waters during the LGM.

The degree of DSi utilization during diatom growth can be calculated using either a closed-system (Rayleigh) or an open-system (steady state) model [e.g., *Beucher et al*., 2007; *Reynolds et al*., 2008] (see section 4.3.1). The continuous supply of DSi from the Asian dust flux (see section 4.4.1) invalidates the premise of closed-system dynamics, making the open-system model more suitable for our calculation. The open-system model describes the evolution of $\delta^{30}Si_{DSi}$ and $\delta^{30}Si_{BSi}$ in the context of a continuous supply of nutrients [*Varela et al*., 2004; *Fry*, 2006]:

$$\delta^{30}Si_{DSi} = \delta^{30}Si_{DSi\,initial} - {}^{30}\varepsilon \times (1 - f) \quad (3)$$

$$\delta^{30}Si_{BSi} = \delta^{30}Si_{DSi\,initial} + {}^{30}\varepsilon \times f \quad (4)$$

where $\delta^{30}Si_{DSi\ initial}$ is the $\delta^{30}Si$ of DSi in surface water prior to biological utilization and f is the fraction of DSi remaining in the surface water after consumption. Therefore, f can be calculated based on measured $\delta^{30}Si_{E.\ rex}$ values and estimates for $\delta^{30}Si_{DSi\ initial}$ (=DSi_{eolian} or $-0.2‰ + \tau$) and ${}^{30}\varepsilon$ (−1.1‰; see section 4.3.1). Assuming that $\tau = 0$‰, the average $\delta^{30}Si_{E.\ rex}$ for cores WPD-03 and WPD-12 (−1.04‰) yields an estimated f of ~76%. If $\tau = -0.3$‰, then the same calculation yields an estimated f of ~49%. These results indicate that *E. rex* consumed only ~24–51% of DSi in EPS surface waters, leaving large quantities of unutilized DSi. These considerations suggest that EPS surface waters were eutrophic with respect to nutrient silicon during the LGM (opposite to the condition of the modern EPS) and that other nutrients were biolimiting. Iron fertilization by Asian dust may have stimulated *E. rex* to consume nitrate and phosphate rapidly [*Takeda*, 1998], making N or P a possible biolimiting nutrient, which will be the subject of future investigations.

4.4.3. Relationship Between DSi Cycle and *E. rex* LDM Formation in the Eastern Philippine Sea

The paleoceanographic conditions of the EPS during the LGM, including the Asian dust flux [*Xiong et al*., 2010, 2013a], redox conditions [*Xiong et al*., 2012a, 2012b], productivity levels [*Xiong et al*., 2012a, 2012b, 2013b], and CO_2 partial pressure of surface water ($pCO_{2\text{-}sw}$) [*Xiong et al*., 2013a], have been investigated previously. In this section, we examine the linkage of the DSi cycle to these paleoceanographic conditions.

During PC deposition, diatom primary production was suppressed, as inferred from extremely low opal concentrations (Figure 4c). Redox conditions were oxic both at the sediment-water interface and in the overlying water column (Figure 8a). During DC deposition, intensification of the EAWM not only carried large amounts of dust (including silicon and iron) to the surface EPS but also resulted in enhanced upwelling of subsurface/intermediate waters. Wind-driven upwelling may have stimulated modest

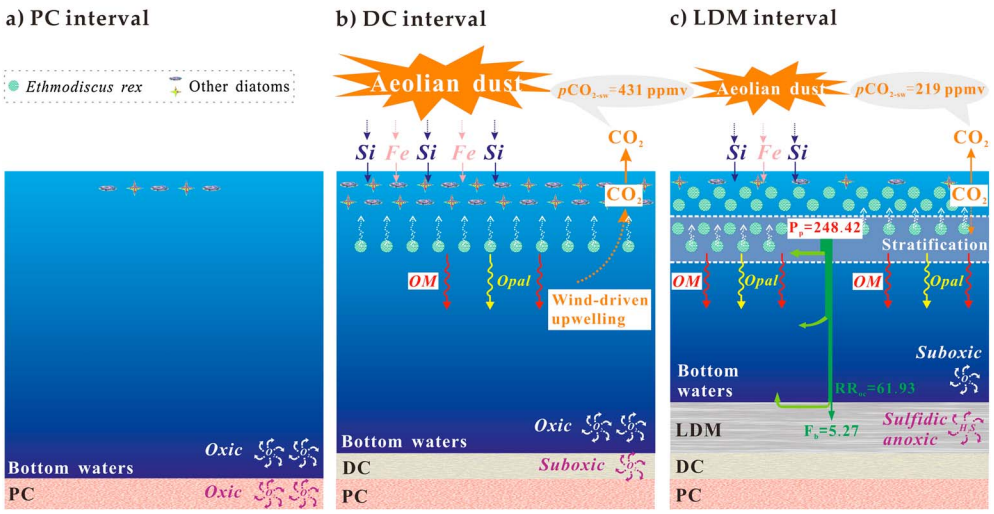

Figure 8. Schematic model of relationship of laminated *E. rex* diatom mat formation to paleoceanographic conditions in the EPS during the LGM: (a) PC interval, (b) DC interval, and (c) LDM interval. Inferred benthic redox conditions are from *Xiong et al.* [2012b]; patterns of dust input, wind-driven upwelling, and thermohaline stratification are from *Xiong et al.* [2010, 2013a]; $pCO_{2\text{-sw}}$ estimates are from *Xiong et al.* [2013a]; and productivity estimates are from *Xiong et al.* [2013b]. In Figures 8a–8c, the number of *E. rex* and other diatoms shown is proportional to their inferred productivity; the number of blue and pink arrows shown is proportional to the magnitudes of the Asian eolian silicon and iron fluxes, respectively; and the number of red and yellow arrows shown is proportional to the magnitudes of organic matter and opal sinking fluxes, respectively. Abbreviations: OM, organic matter; $pCO_{2\text{-sw}}$, CO_2 partial pressure of the study area surface waters; P_p, primary productivity; RR_{oc}, rain rate of organic carbon; F_b, burial flux of organic carbon; LDM, laminated *E. rex* diatom mats; DC, diatomaceous clay; and PC, pelagic clay. See section 4.4.3 for further explanation.

increases of productivity among small spring-bloom diatoms. The DSi and dissolved iron derived from Asian dust inputs would have been rapidly consumed by these diatoms. *E. rex* could not have bloomed massively during this interval due to its requirement for water mass stratification [*Gingele and Schmieder*, 2001; *De Deckker and Gingele*, 2002; *Kemp and Villareal*, 2013] (see section 4.4.1). Modestly higher organic matter sinking fluxes resulted in a shift from oxic to suboxic conditions at the sediment-water interface, but the overlying water column remained oxic. Intensified upwelling brought high concentrations of deep CO_2 to the surface ($pCO_{2\text{-sw}} = 431$ ppmv) [*Xiong et al.*, 2013a], causing the EPS to act as a strong CO_2 source to the atmosphere (Figure 8b).

During LDM deposition, a weakening of the EAWM terminated upwelling and led to sustained stratification of the EPS [*Xiong et al.*, 2010, 2013a]. Although the Asian dust flux decreased at the same time, it remained sufficiently high as to still supply abundant DSi_{eolian} and dissolved iron to EPS surface waters. A combination of surface stratification and high DSi_{eolian} availability induced strong annual blooms of *E. rex*. Productivity by *E. rex* resulted in a substantial export flux of organic carbon and opal through the "fall dump" [*Kemp et al.*, 2000; *Kemp and Villareal*, 2013], with estimated average organic productivity of 248.42 g m^{-2} yr^{-1} [*Xiong et al.*, 2013b]. However, the rain rate and burial flux of organic carbon were very low, with estimated averages of 61.93 g m^{-2} yr^{-1} and 5.27 g m^{-2} yr^{-1}, respectively [*Xiong et al.*, 2013b]. These observations indicate that remineralization of organic matter was intense owing to high levels of dissolved oxygen in the water column and, frequently, in sediment pore waters. High respiratory oxygen demand, in combination with surface stratification, eventually resulted in sulfidic-anoxic conditions at the sediment-water interface and mainly suboxic conditions in the deeper part of the water column. High productivity, in combination with isolation of remineralized CO_2 through stratification, resulted in a decrease in average surface $pCO_{2\text{-sw}}$ to 219 ppmv, converting the surface EPS from a source to a weak sink for CO_2 during LDM deposition [*Xiong et al.*, 2013a] (Figure 8c).

4.4.4. Implications for *E. rex* LDM Formation in World Ocean

Both the ocean stratification model and frontal zone model propose that *E. rex* utilizes nutrients from subsurface waters (i.e., the ocean interior) to sustain blooms [*Villareal et al.*, 1999a; *Yoder et al.*, 1994; *Kemp et al.*, 2000, 2006; *Kemp and Villareal*, 2013]. However, our results suggest that *E. rex* can also use surface

water DSi derived from eolian dust (i.e., a source external to the ocean). These observations are also consistent with modern measurements in the central North Pacific gyre, where *E. rex* acquires DSi from surface rather than deep waters [*Villareal et al.*, 1999a]. Other giant diatom species, e.g., *Rhizosolenia* spp. in the central North Pacific, are also known to utilize DSi from the euphotic zone without any DSi uptake at depth [*Shipe et al.*, 1999]. Our data coupled with modern observations indicate that giant diatoms do not always rely on buoyancy regulation to obtain nutrients from below the nutricline [*Villareal*, 1992; *Villareal and Carpenter*, 1994]. In summary, our research provides a new model for formation of *E. rex* LDMs.

5. Conclusions

1. *E. rex* blooms in the eastern Philippine Sea (EPS) during the Last Glacial Maximum (LGM) show a unique silicon isotopic composition that is markedly more ^{30}Si depleted ($\delta^{30}Si_{E.\ rex} = -1.23‰$ to $-0.83‰$; average $-1.04‰$) than known diatom deposits of any age.
2. A binary mixing model, utilizing estimated δ^{30}Si for upwelled silicon versus eolian silicon end-members, was constructed to evaluate DSi sources for these *E. rex* blooms. To sustain blooms in the EPS during the LGM, *E. rex* utilized DSi primarily from dissolution of continuously supplied Asian dust and only to a minor extent from upwelling of subsurface and intermediate waters sourced from SAMW, AAIW, and NPIW. *E. rex* utilized an estimated ~24–51% of the DSi in EPS surface waters, reflecting eutrophic conditions relative to nutrient silicon during the LGM.
3. The DSi cycle is consistent with paleoceanographic conditions during LDM deposition. High levels of DSi generated through dissolution of Asian dust constantly transported to the EPS induced massive blooms of *E. rex* that led to LDM formation. High *E. rex* primary productivity and export productivity converted surface waters of the EPS from a strong CO_2 source to a weak CO_2 sink and caused deepwater redox conditions to shift from oxic to mainly suboxic.
4. Our results suggest that buoyancy regulation with extraction of nutrients from below the nutricline is not the sole nutrient utilization pathway for giant diatoms. *E. rex* can also utilize DSi generated through dissolution of eolian dust. The "eolian-silicon-induced bloom" model represents an important new addition to mechanisms of formation of *E. rex* LDMs.

Acknowledgments
The data for this paper are available on request from the first author (Z. Xiong, zhfxiong@qdio.ac.cn). Research by T.L. is supported by the Strategic Priority Research Program of the Chinese Academy of Sciences (grant XDA11030104), National Program on Global Change and Air-Sea Interaction (grant GASI-04-01-02), and National Natural Science Foundation of China (NSFC) (grants 41230959 and 40776031). Research by Z.X. is supported by NSFC (grant 41106042) and Open Fund of the Key Laboratory of Marine Geology and Environment, China Academy of Sciences (grant MGE2011KG03). Research by T.J.A. is supported by the Sedimentary Geology and Paleobiology program of the U.S. National Science Foundation, the NASA Exobiology program, and the China University of Geosciences-Wuhan (programs GPMR201301 and BGL21407 from the State Key Laboratories of GPMR and BGEG). Research by K.D. is supported through SFB 754 funded by the German Science Foundation, to which this paper is a contribution. Research by S.O. is supported by the FNRS, Belgium. Research by B.Z. is supported by NSFC (grant 41006032). Many thanks to Janice Jones for her help with diatom silicon isotope analysis at the UCSB. We also appreciate the constructive comments from the Editor Christopher Charles, Kate Hendry, and an anonymous reviewer.

References

Abrantes, F. (2001), Assessing the *Ethmodiscus* ooze problem: New perspective from a study of an eastern equatorial core, *Deep Sea Res., Part I*, *48*, 125–135.

Albarède, F., P. Telouk, J. Blichert-Toft, M. Boyet, A. Agranier, and B. Nelson (2004), Precise and accurate isotopic measurements using multiple-collector ICPMS, *Geochim. Cosmochim. Acta*, *68*, 2725–2744.

Alleman, L. Y., D. Cardinal, C. Cocquyt, P. D. Plisnier, J. P. Descy, I. Kimirei, D. Sinyinza, and L. André (2005), Silicon isotopic fractionation in Lake Tanganyika and its tributaries, *J. Great Lakes Res.*, *31*, 509–519.

Arellano-Torres, E., L. E. Pichevin, and R. S. Ganeshram (2011), High-resolution opal records from the eastern tropical Pacific provide evidence for silicic acid leakage from HNLC regions during glacial periods, *Quat. Sci. Rev.*, *30*, 1112–1121.

Beucher, C. P., M. A. Brzezinski, and X. Crosta (2007), Silicic acid dynamics in the glacial sub-Antarctic: Implications for the silicic acid leakage hypothesis, *Global Biogeochem. Cycles*, *21*, GB3015, doi:10.1029/2006GB002746.

Beucher, C. P., M. A. Brzezinski, and J. L. Jones (2008), Sources and biological fractionation of silicon isotopes in the eastern equatorial Pacific, *Geochim. Cosmochim. Acta*, *72*, 3063–3073.

Beucher, C. P., M. A. Brzezinski, and J. L. Jones (2011), Mechanisms controlling silicon isotope distribution in the eastern equatorial Pacific, *Geochim. Cosmochim. Acta*, *75*, 4286–4294.

Bingham, F. M., and R. Lukas (1995), The distribution of intermediate water in the western equatorial Pacific during January-February 1986, *Deep Sea Res., Part II*, *42*, 1545–1573.

Bodén, P., and J. Backman (1996), A laminated sediment sequence from northern North Atlantic Ocean and its climatic record, *Geology*, *24*, 507–510.

Bory, A. J.-M., P. E. Biscaye, and F. E. Grousset (2003), Two distinct seasonal Asian source regions for mineral dust deposited in Greenland (NorthGRIP), *Geophys. Res. Lett.*, *30*(4), 1167, doi:10.1029/2002GL016446.

Bostock, H. C., B. N. Opdyke, and M. J. M. Williams (2010), Characterising the intermediate depth waters of the Pacific Ocean using δ^{13}C and other geochemical tracers, *Deep Sea Res., Part I*, *57*, 847–859.

Bradtmiller, L. I., R. F. Anderson, M. Q. Fleisher, and L. H. Burckle (2007), Opal burial in the equatorial Atlantic Ocean over the last 30 ka: Implications for glacial-interglacial changes in the ocean silicon cycle, *Paleoceanography*, *22*, PA4216, doi:10.1029/2007PA001443.

Brzezinski, M. A., C. J. Pride, V. M. Franck, D. M. Sigman, J. L. Sarmiento, K. Matsumoto, N. Gruber, G. H. Rau, and K. H. Coale (2002), A switch from $Si(OH)_4$ to NO_3^- depletion in the glacial Southern Ocean, *Geophys. Res. Lett.*, *29*(12, 1564), doi:10.1029/2001GL014349.

Brzezinski, M. A., J. L. Jones, C. P. Beucher, and M. S. Demarest (2006), Automated determination of silicon isotope natural abundance by the acid decomposition of cesium hexafluosilicate, *Anal. Chem.*, *78*, 6109–6114.

Bukry, D. (1974), Coccolith and silicoflagellate stratigraphy, eastern Indian Ocean, Deep Sea Drilling Project Leg 22, in *Initial Reports of the Deep Sea Drilling Project*, vol. 22, edited by C. C. von der Borch et al., pp. 601–607, U.S. Gov. Print. Off., Washington, D. C.

Cao, Z., M. Frank, M. Dai, P. Grasse, and C. Ehlert (2012), Silicon isotope constraints on sources and utilization of silicic acid in the northern South China Sea, *Geochim. Cosmochim. Acta*, *97*, 88–104.

Cardinal, D., L. Y. Alleman, F. Dehairs, N. Savoye, T. W. Trull, and L. André (2005), Relevance of silicon isotopes to Si-nutrient utilization and Si-source assessment in Antarctic waters, *Global Biogeochem. Cycles*, *19*, GB2007, doi:10.1029/2004GB002364.
Cardinal, D., N. Savoye, T. W. Trull, F. Dehairs, E. E. Kopczynska, F. Fripiat, J. L. Tison, and L. André (2007), Silicon isotopes in spring Southern Ocean diatoms: Large zonal changes despite homogeneity among size fractions, *Mar. Chem.*, *106*, 46–62.
Carpenter, E. J., J. P. Montoya, J. Burns, M. R. Mulholland, A. Subramaniam, and D. G. Capone (1999), Extensive bloom of a N_2-fixing diatom/cyanobacterial association in the tropical Atlantic Ocean, *Mar. Ecol. Prog. Ser.*, *185*, 273–283.
Chiang, J. C. H. (2009), The tropics in paleoclimate, *Annu. Rev. Earth Planet. Sci.*, *37*, 263–297.
Cornelis, J.-T., D. Weis, L. Lavkulich, M.-L. Vermeire, B. Delvaux, and J. Barling (2014), Silicon isotopes record dissolution and re-precipitation of pedogenic clay minerals in a podzolic soil chronosequence, *Geoderma*, *235–236*, 19–29.
Crosta, X., and N. Koç (2007), Diatoms: From micropaleontology to isotope geochemistry, in *Proxies in Late Cenozoic Paleoceanography*, *Developments in Marine Geology Series*, vol. 1, edited by C. Hilaire-Marcel and A. de Vernal, pp. 327–369, Elsevier, Amsterdam.
Crosta, X., C. Beucher, K. Pahnke, and M. A. Brzezinski (2007), Silicic acid leakage from the Southern Ocean: Opposing effects of nutrient uptake and oceanic circulation, *Geophys. Res. Lett.*, *34*, L13601, doi:10.1029/2006GL029083.
De Deckker, P., and F. X. Gingele (2002), On the occurrence of the giant diatom *Ethmodiscus rex* in an 80-ka record from a deep-sea core, southeast of Sumatra, Indonesia: Implications for tropical oceanography, *Mar. Geol.*, *183*, 31–43.
De La Rocha, C. L. (2003), Silicon isotope fractionation by marine sponges and the reconstruction of the silicon isotope composition of ancient deep water, *Geology*, *31*, 423–426.
De La Rocha, C. L. (2006), Opal-based isotopic proxies of paleoenvironmental conditions, *Global Biogeochem. Cycles*, *20*, GB4S09, doi:10.1029/2005GB002664.
De La Rocha, C. L., and M. J. Bickle (2005), Sensitivity of silicon isotopes to whole-ocean changes in the silica cycle, *Mar. Geol.*, *217*, 267–282.
De La Rocha, C. L., M. A. Breszinski, and M. J. DeNiro (1997), Fractionation of silicon isotopes by marine diatoms during biogenic silica formation, *Geochim. Cosmochim. Acta*, *61*, 5051–5056.
De La Rocha, C. L., M. A. Brzezinski, M. DeNiro, and A. Shemesh (1998), Silicon-isotope composition of diatoms as an indicator of past oceanic change, *Nature*, *395*, 680–683.
De La Rocha, C. L., M. A. Brzezinski, and M. J. DeNiro (2000), A first look at the distribution of the stable isotopes of silicon in natural waters, *Geochim. Cosmochim. Acta*, *64*, 2467–2477.
De La Rocha, C. L., P. Bescont, A. Croguennoc, and E. Ponzevera (2011), The silicon isotopic composition of surface waters in the Atlantic and Indian sectors of the Southern Ocean, *Geochim. Cosmochim. Acta*, *75*, 5283–5295.
de Souza, G. F., B. C. Reynolds, G. C. Johnson, J. L. Bullister, and B. Bourdon (2012a), Silicon stable isotope distribution traces Southern Ocean export of Si to the eastern South Pacific thermocline, *Biogeosciences*, *9*, 4199–4213.
de Souza, G. F., B. C. Reynolds, J. Rickli, M. Frank, M. A. Saito, L. J. A. Gerringa, and B. Bourdon (2012b), Southern Ocean control of silicon stable isotope distribution in the deep Atlantic Ocean, *Global Biogeochem. Cycles*, *26*, GB2035, doi:10.1029/2011GB004141.
Demarest, M. S., M. A. Brzezinski, and C. P. Beucher (2009), Fractionation of silicon isotopes during biogenic silica dissolution, *Geochim. Cosmochim. Acta*, *73*, 5572–5583.
Ding, T., S. Jiang, D. Wan, Y. Li, J. Li, H. Song, Z. Liu, and X. Yao (1996), *Silicon Isotope Geochemistry*, Geological House, Beijing.
Dubois, N., M. Kienast, S. Kienast, S. E. Calvert, R. François, and R. F. Anderson (2010), Sedimentary opal records in the eastern equatorial Pacific: It is not all about leakage, *Global Biogeochem. Cycles*, *24*, GB4020, doi:10.1029/2010GB003821.
Duce, R. A., et al. (1991), The atmospheric input of trace species to the world ocean, *Global Biogeochem. Cycles*, *5*, 193–259.
Egan, K. E., R. E. M. Rickaby, M. J. Leng, K. R. Hendry, M. Hermoso, H. J. Sloane, H. C. Bostock, and A. N. Halliday (2012), Diatom silicon isotopes as a proxy for silicic acid utilisation: A Southern Ocean core top calibration, *Geochim. Cosmochim. Acta*, *96*, 174–192.
Egan, K. E., R. E. M. Rickaby, K. R. Hendry, and A. N. Halliday (2013), Opening the gateways for diatoms primes Earth for Antarctic glaciations, *Earth Planet. Sci. Lett.*, *375*, 34–43.
Ehlert, C., P. Grasse, E. Mollier-Vogel, T. Böschen, J. Franz, G. F. de Souza, B. C. Reynolds, L. Stramma, and M. Frank (2012), Factors controlling the silicon isotope distribution in waters and surface sediments of the Peruvian coastal upwelling, *Geochim. Cosmochim. Acta*, *99*, 128–145.
Ehlert, C., P. Grasse, and M. Frank (2013), Changes in silicate utilisation and upwelling intensity off Peru since the Last Glacial Maximum—Insights from silicon and neodymium isotopes, *Quat. Sci. Rev.*, *2*, 18–35.
Ellwood, M. J., M. Wille, and W. Maher (2010), Glacial silicic acid concentrations in the Southern Ocean, *Science*, *330*, 1088–1091.
Etourneau, J., C. Ehlert, M. Frank, P. Martinez, and R. Schneider (2012), Contribution of changes in opal productivity and nutrient distribution in the coastal upwelling systems to late Pliocene/early Pleistocene climate cooling, *Clim. Past*, *8*, 1435–1445.
Fine, R. A., R. Lukas, F. M. Bingham, M. J. Warner, and R. H. Gammon (1994), The western equatorial Pacific: A water mass crossroads, *J. Geophys. Res.*, *99*, 25,063–25,080, doi:10.1029/94JC02277.
Firing, E., S. E. Wijffels, and P. Hacker (1998), Equatorial subthermocline currents across the Pacific, *J. Geophys. Res.*, *103*, 21,413–21,423, doi:10.1029/98JC01944.
Fripiat, F. (2010), Isotopic approaches of the silicon cycle: The Southern Ocean case study, PhD thesis, Université Libre de Bruxelles, Brussels, Belgium.
Fripiat, F., D. Cardinal, J.-L. Tison, A. Worby, and L. André (2007), Diatom-induced silicon isotopic fractionation in Antarctic sea ice, *J. Geophys. Res.*, *112*, G02001, doi:10.1029/2006JG000244.
Fripiat, F., A. J. Cavagna, F. Dehairs, S. Speich, L. André, and D. Cardinal (2011a), Silicon pool dynamics and biogenic silica export in the Southern Ocean inferred from Si-isotopes, *Ocean Sci.*, *7*, 533–547.
Fripiat, F., A. J. Cavagna, N. Savoye, F. Dehairs, L. André, and D. Cardinal (2011b), Isotopic constraints on the Si-biogeochemical cycle of the Antarctic Zone in the Kerguelen area (KEOPS), *Mar. Chem.*, *123*, 11–22.
Fripiat, F., A. J. Cavagna, F. Dehairs, A. de Brauwere, L. André, and D. Cardinal (2012), Processes controlling the Si-isotopic composition in the Southern Ocean and application for paleoceanography, *Biogeosciences*, *9*, 2443–2457.
Fry, B. (2006), *Stable Isotope Ecology*, Springer, New York.
Gao, Y., J. R. Anderson, and X. Hua (2007), Dust characteristics over the North Pacific observed through shipboard measurements during the ACE-Asia experiment, *Atmos. Environ.*, *41*, 7907–7922.
Gardner, J. V., and L. H. Burckle (1975), Upper Pleistocene *Ethmodiscus rex* oozes from the eastern equatorial Atlantic, *Micropaleontology*, *21*, 236–242.
Georg, R. B., B. C. Reynolds, M. Frank, and A. N. Halliday (2006a), Mechanisms controlling the silicon isotopic compositions of river waters, *Earth Planet. Sci. Lett.*, *249*, 290–306.
Georg, R. B., B. C. Reynolds, M. Frank, and A. N. Halliday (2006b), New sample preparation techniques for the determination of Si isotopic compositions using MC-ICPMS, *Chem. Geol.*, *235*, 95–104.

Georg, R. B., A. J. West, A. R. Basu, and A. N. Halliday (2009), Silicon fluxes and isotope composition of direct ground water discharge into the Bay of Bengal and the effect on the global ocean silicon isotope budget, *Earth Planet. Sci. Lett.*, *283*, 67–74.
Gingele, F. X., and F. Schmieder (2001), Anomalous South Atlantic lithologies confirm global scales of unusual mid-Pleistocene climate excursion, *Earth Planet. Sci. Lett.*, *186*, 93–101.
Goldman, J. C. (1993), Potential role of large oceanic diatoms in new primary production, *Deep Sea Res., Part I*, *40*, 159–168.
Goldman, J. C., and D. J. McGillicuddy Jr. (2003), Effect of large marine diatoms growing at low light on episodic new production, *Limnol. Oceanogr.*, *48*, 1176–1182.
Gombos, A. M., Jr. (1984), Late Neogene diatoms and diatom oozes in the Central South Atlantic, in *Initial Reports of the Deep Sea Drilling Project*, vol. 73, edited by K. J. Hsü et al., pp. 487–494, U.S. Gov. Print. Off., Washington, D. C.
Grasse, P., C. Ehlert, and M. Frank (2013), The influence of water mass mixing on the dissolved silicon isotope composition of the eastern equatorial Pacific, *Earth Planet. Sci. Lett.*, *380*, 60–71.
Grasshoff, K., K. Kremling, and M. Ehrhardt (1999), *Methods of Sweater Analysis*, 3rd ed., John Wiley, New York.
Harrison, K. (2000), Role of increased marine silica input on paleo-pCO_2 levels, *Paleoceanography*, *15*, 292–298, doi:10.1029/1999PA000427.
Hendry, K. R., and L. F. Robinson (2012), The relationship between silicon isotope fractionation in sponges and silicic acid concentration: Modern and core-top studies of biogenic opal, *Geochim. Cosmochim. Acta*, *81*, 1–12.
Hendry, K. R., and M. A. Brzezinski (2014), Using silicon isotopes to understand the role of the Southern Ocean in modern and ancient biogeochemistry and climate, *Quat. Sci. Rev.*, *89*, 13–26.
Hendry, K. R., M. J. Leng, L. F. Robinson, H. J. Sloane, J. Blusztjan, R. E. M. Rickaby, R. B. Georg, and A. N. Halliday (2011), Silicon isotopes in Antarctic sponges: An interlaboratory comparison, *Antarct. Sci.*, *23*, 34–42.
Hendry, K. R., L. F. Robinson, J. F. McManus, and J. D. Hays (2014), Silicon isotopes indicate enhanced carbon export efficiency in the North Atlantic during deglaciation, *Nat. Commun.*, *5*, 3107, doi:10.1038/ncomms4107.
Horn, M. G., C. P. Beucher, R. S. Robinson, and M. A. Brzezinski (2011), Southern ocean nitrogen and silicon dynamics during the last deglaciation, *Earth Planet. Sci. Lett.*, *310*, 334–339.
Jiang, F., T. Li, Z. Xu, A. Li, M. Frank, and T. Chen (2013), Asian dust input in the western Philippine Sea: Evidence from radiogenic Sr and Nd isotopes, *Geochem. Geophys. Geosyst.*, *14*, 1538–1551, doi:10.1002/ggge.20116.
Kawabe, M., and S. Fujio (2010), Pacific Ocean circulation based on observation, *J. Oceanogr.*, *66*, 389–403.
Kawahata, H., T. Okamoto, E. Matsumoto, and H. Ujiie (2000), Fluctuations of eolian flux and ocean productivity in the mid-latitude North Pacific during the last 200 kyr, *Quat. Sci. Rev.*, *19*, 1279–1291.
Kemp, A. E. S., and J. G. Baldauf (1993), Vast Neogene laminated diatom mat deposits from the eastern equatorial Pacific Ocean, *Nature*, *362*, 141–143.
Kemp, A. E. S., and T. A. Villareal (2013), High diatom production and export in stratified waters—A potential negative feedback to global warming, *Prog. Oceanogr.*, *119*, 4–23.
Kemp, A. E. S., J. Pike, R. B. Pearce, and C. B. Lange (2000), The "fall dump"—A new perspective on the role of a "shade flora" in the annual cycle of diatom production and exportation, *Deep Sea Res., Part II*, *47*, 2129–2154.
Kemp, A. E. S., R. B. Pearce, I. Grigorov, J. Rance, C. B. Lange, P. Quilty, and I. Salter (2006), Production of giant marine diatoms and their export at oceanic frontal zones: Implications for Si and C flux from stratified oceans, *Global Biogeochem. Cycles*, *20*, GB4S04, doi:10.1029/2006GB002698.
Kemp, A. E. S., I. Grigorov, R. B. Pearce, and A. C. Naveira Garabato (2010), Migration of the Antarctic Polar Front through the mid-Pleistocene transition: Evidence and climatic implications, *Quat. Sci. Rev.*, *29*, 1993–2009.
Kienast, S. S., M. Kienast, S. Jaccard, S. E. Calvert, and R. François (2006), Testing the silicic acid leakage hypothesis with sedimentary opal records from the eastern equatorial Pacific over the last 150 kyrs, *Geophys. Res. Lett.*, *33*, L15607, doi:10.1029/2006GL026651.
Kohfeld, K. E., and S. P. Harrison (2001), DIRTMAP: The geological record of dust, *Earth Sci. Rev.*, *54*, 81–114.
Leng, M. J., G. E. A. Swann, M. J. Hodson, J. J. Tyler, S. V. Patwardhan, and H. J. Sloane (2009), The potential use of silicon isotope composition of biogenica silica as a proxy for environmental change, *Silicon*, *1*, 65–77.
Li, T., T. Masuzawa, and H. Kitagawa (2004), Seasonal variations in settling fluxes of major components in the oligotrophic Shikoku Basin, the western North Pacific: Coincidence of high biogenic flux with Asian dust supply in spring, *Mar. Chem.*, *91*, 187–210.
Maher, B. A., J. M. Prospero, D. Mackie, D. Gaiero, P. P. Hesse, and Y. Balkanski (2010), Global connections between aeolian dust, climate and ocean biogeochemistry at the present day and at the Last Glacial Maximum, *Earth Sci. Rev.*, *99*, 61–97.
Maier, E., B. Chapligin, A. Abelmann, R. Gersonde, O. Esper, J. Ren, H. Friedrichsen, H. Meyer, and R. Tiedemann (2013), Combined oxygen and silicon isotope analysis of diatom silica from a deglacial subarctic Pacific record, *J. Quat. Sci.*, *28*, 571–581.
Marinov, I., A. Gnanadesikan, J. R. Toggweiler, and J. L. Sarmiento (2006), The Southern Ocean biogeochemical divide, *Nature*, *441*, 964–967.
Maslin, M. A., and G. A. Swann (2006), Isotopes in marine sediments, in *Isotopes in Paleoenvironmental Research*, vol. 10, edited by P. A. Leng, pp. 227–290, Springer, Dordrecht, Netherlands.
Matsumoto, K., J. L. Sarmiento, and M. A. Brzezinski (2002), Silicic acid leakage from the Southern Ocean: A possible explanation for glacial atmospheric pCO_2, *Global Biogeochem. Cycles*, *16*(3, 1031), doi:10.1029/2001GB001442.
McKendry, I. G., J. P. Hacker, R. Stull, S. Sakiyama, D. Mignacca, and K. Reid (2001), Long-range transport of Asian dust to the Lower Fraser Valley, British Columbia, Canada, *J. Geophys. Res.*, *106*, 18,361–18,370.
Mikkelsen, N. (1977), On the origin of *Ethmodiscus* ooze, *Mar. Micropaleontol.*, *2*, 35–46.
Milligan, A. J., D. E. Varela, M. A. Brzezinski, and F. M. M. Morel (2004), Dynamics of silicon metabolism and silicon isotopic discrimination in a marine diatom as a function of pCO_2, *Limnol. Oceanogr.*, *49*, 322–329.
Muhs, D. R. (2013), The geological records of dust in the Quaternary, *Aeolian Res.*, *9*, 3–48.
Nilson, E., and F. Lehmkuhl (2001), Interpreting temporal patterns in the late Quaternary dust flux from Asian to the North Pacific, *Quat. Int.*, *76–77*, 67–76.
Nozaki, Y., and Y. Yamamoto (2001), Radium 228 based nitrate fluxes in the eastern Indian Ocean and the South China Sea and a silicon-induced "alkalinity pump" hypothesis, *Global Biogeochem. Cycles*, *15*, 555–567, doi:10.1029/2000GB001309.
Opfergelt, S., and P. Delmelle (2012), Silicon isotopes and continental weathering processes: Assessing controls on Si transfer to the ocean, *C. R. Geosci.*, *344*, 723–738.
Panizzo, V., J. Crespin, X. Crosta, A. Shemesh, G. Massé, R. Yam, N. Mattielli, and D. Cardinal (2014), Sea ice diatom contributions to Holocene nutrient utilization in East Antarctica, *Paleoceanography*, *29*, 328–343, doi:10.1002/2014PA002609.
Pichevin, L. E., B. C. Reynolds, R. S. Ganeshram, I. Cacho, L. D. Pena, K. Keefe, and R. M. Ellam (2009), Enhanced carbon pump inferred from relaxation of nutrient imitation in the glacial ocean, *Nature*, *459*, 1114–1117.
Pichevin, L. E., R. S. Ganeshram, B. C. Reynolds, F. Prahl, T. F. Pedersen, R. Thunell, and E. L. McClymont (2012), Silicic acid biogeochemistry in the Gulf of California: Insights from sedimentary Si isotopes, *Paleoceanography*, *27*, PA2201, doi:10.1029/2011PA002237.

Pike, J. (2000), Backscattered electron imagery analysis of early Pliocene laminated *Ethmodiscus* ooze, Site 1010, in *Proceedings of the Ocean Drilling Program*, Scientific Results, vol. 167, edited by M. Lyle et al., pp. 207–212, Ocean Drilling Program, College Station, Tex.
Qu, T., and E. J. Lindstrom (2004), Northward intrusion of Antarctic Intermediate Water in the western Pacific, *J. Phys. Oceanogr.*, *34*, 2104–2118.
Qu, T., H. Mitsudera, and T. Yamagata (1999), A climatology of the circulation and water mass distribution near the Philippine Coast, *J. Phys. Oceanogr.*, *29*, 1488–1505.
Rackebrandt, N., H. Kuhnert, J. Groeneveld, and T. Bickert (2011), Persisting maximum Agulhas leakage during MIS 14 indicated by massive *Ethmodiscus* oozes in the subtropical South Atlantic, *Paleoceanography*, *26*, PA3202, doi:10.1029/2010PA001990.
Ragueneau, O., et al. (2000), A review of the Si cycle in the modern ocean: Recent progress and missing gaps in the application of biogenic opal as a paleoproductivity proxy, *Global Planet. Change*, *26*, 317–365.
Rea, D. K. (2007), Eolian records, deep-sea sediments, in *The Encyclopedia of Quaternary Sciences*, edited by S. A. Elias, pp. 643–650, Elsevier, Amsterdam.
Reynolds, B. C. (2009), Modeling the modern marine δ^{30}Si distribution, *Global Planet. Change*, *23*, GB2015, doi:10.1029/2008GB003266.
Reynolds, B. C., M. Frank, and A. N. Halliday (2006), Silicon isotope fractionation during nutrient utilization in the North Pacific, *Earth Planet. Sci. Lett.*, *244*, 431–443.
Reynolds, B. C., et al. (2007), An interlaboratory comparison of Si isotope reference materials, *J. Anal. Atom. Spectrom.*, *22*, 561–568.
Reynolds, B. C., M. Frank, and A. N. Halliday (2008), Evidence for a major change in silicon cycling in the subarctic North Pacific at 2.73 Ma, *Paleoceanography*, *23*, PA4219, doi:10.1029/2007PA001563.
Romero, O., and F. Schmieder (2006), Occurrence of thick *Ethmodiscus* oozes associated with a terminal mid-Pleistocene Transition event in the oligotrophic subtropical South Atlantic, *Palaeogeogr. Palaeoclimatol. Palaeoecol.*, *235*, 321–329.
Romero, O., G. E. A. Swann, D. A. Hodell, P. Helmke, D. Rey, and B. Rubio (2011), A highly productive subarctic Atlantic during the Last Interglacial and the role of diatoms, *Geology*, *39*, 1015–1018.
Rose, K. A., E. L. Sikes, T. P. Guilderson, P. Shane, T. M. Hill, R. Zahn, and H. J. Spero (2010), Upper-ocean-to-atmosphere radiocarbon offsets imply fast deglacial carbon dioxide release, *Nature*, *466*, 1093–1097.
Sarmiento, J. L., N. Gruber, M. A. Brzezinski, and J. P. Dunne (2004), High-latitude controls of thermocline nutrients and low latitude biological productivity, *Nature*, *427*, 56–60.
Sarmiento, J. L., J. Simeon, A. Gnanadesikan, N. Gruber, R. M. Key, and R. Schlitzer (2007), Deep ocean biogeochemistry of silicic acid and nitrate, *Global Planet. Change*, *21*, GB1S90, doi:10.1029/2006GB002720.
Savage, P. S., R. B. Georg, H. M. Williams, and A. N. Halliday (2013), The silicon isotope composition of the upper continental crust, *Geochim. Cosmochim. Acta*, *109*, 384–399.
Schlitzer, R. (2000), Electronic atlas of WOCE hydrographic and tracer data now available, *Eos Trans. AGU*, *81*, 45, doi:10.1029/00EO00028.
Scholz, F., C. Hensen, M. Schmidt, and J. Geersen (2013), Submarine weathering of silicate minerals and the extent of pore water freshening at active continental margins, *Geochim. Cosmochim. Acta*, *100*, 200–216.
Schrader, H. J. (1974), Cenozoic marine planktonic diatom stratigraphy of the tropical Indian Ocean, in *Initial Reports of the Deep Sea Drilling Project*, vol. 24, edited by R. L. Fischer et al., pp. 887–967, U.S. Gov. Print. Off., Washington, D. C.
Shao, Y., K.-H. Wyrwoll, A. Chappell, J. Huang, Z. Lin, G. McTainsh, M. Mikami, T. Tanaka, X. Wang, and S. Yoon (2011), Dust cycle: An emerging core theme in Earth system science, *Aeolian Res.*, *2*, 181–204.
Shipe, R. F., M. A. Brzezinski, C. Pilskaln, and T. A. Villareal (1999), *Rhizosolenia* mats: An overlooked source of silica production in the open sea, *Limnol. Oceanogr.*, *44*, 1282–1292.
Siedler, G., J. Holfort, W. Zenk, T. J. Müller, and T. Csernok (2004), Deep-water flow in the Mariana and Caroline Basins, *J. Phys. Oceanogr.*, *34*, 566–581.
Singh, S. P., S. K. Singh, R. Bhushan, and V. K. Rai (2015), Dissolved silicon and its isotopes in the water column of the Bay of Bengal: Internal cycling versus lateral transport, *Geochim. Cosmochim. Acta*, *151*, 172–191.
Stabell, B. (1986), Variations of diatom flux in the eastern equatorial Atlantic during the last 400,000 years ("Meteor" cores 13519 and 13521), *Mar. Geol.*, *72*, 305–323.
Stott, L., C. Poulsen, S. Lund, and R. Thunell (2002), Super ENSO and global climate oscillations at millennial time scales, *Science*, *297*, 222–226.
Sun, X., P. Andersson, C. Humborg, B. Gustafsson, D. J. Conley, P. Crill, and C. M. Mörth (2011), Climate dependent diatom production is preserved in biogenic Si isotope signatures, *Biogeosciences*, *8*, 3491–3499.
Sutton, J. N., D. E. Varela, M. A. Brzezinski, and C. P. Beucher (2013), Species-dependent silicon isotope fractionation by marine diatoms, *Geochim. Cosmochim. Acta*, *104*, 300–309.
Takeda, S. (1998), Influence of iron availability on nutrient consumption ration of diatoms in oceanic waters, *Nature*, *393*, 774–777.
Toggweiler, J. R., K. Dixon, and W. S. Broecker (1991), The Peru upwelling and the ventilation of the South Pacific thermocline, *J. Geophys. Res.*, *96*, 20,467–20,497, doi:10.1029/91JC02063.
Tréguer, P., and C. L. De La Rocha (2013), The world ocean silica cycle, *Annu. Rev. Mar. Sci.*, *5*, 477–501.
Tréguer, P., D. M. Nelson, A. J. van Bennekom, D. J. DeMaster, A. Leynaert, and B. Quéguiner (1995), The balance of silica in the world ocean: A re-estimate, *Science*, *268*, 375–379.
Tsunogai, S. (2002), The western North Pacific playing a key role in global biogeochemical fluxes, *J. Oceanogr.*, *58*, 245–257.
Uno, I., K. Eguchi, K. Yumimoto, T. Takemura, A. Ahimizu, M. Uematsu, Z. Liu, Z. Wang, Y. Hara, and N. Sugimoto (2009), Asian dust transported one full circuit around the globe, *Nat. Geosci.*, *2*, 557–560.
Varela, D. E., C. J. Pride, and M. A. Brzezinshi (2004), Biological fractionation of silicon isotopes in Southern Ocean surface waters, *Global Planet. Change*, *18*, GB1047, doi:10.1029/2003GB002140.
Villareal, T. A. (1991), Nitrogen-fixation by the cyanobacterial symbiont of the diatom genus Hemiaulus, *Mar. Ecol. Prog. Ser.*, *76*, 201–204.
Villareal, T. A. (1992), Buoyancy properties of the giant diatom *Ethmodiscus*, *J. Plankton Res.*, *14*, 459–463.
Villareal, T. A., and E. J. Carpenter (1994), Chemical composition and photosynthetic characteristics of *Ethmodiscus rex* (Bacillariophyceae): Evidence for vertical migration, *J. Phycol.*, *30*, 1–8.
Villareal, T. A., M. A. Altabet, and K. Culver-Rymsza (1993), Nitrogen transport by vertically migrating diatom mats in the North Pacific Ocean, *Nature*, *363*, 709–712.
Villareal, T. A., L. Joseph, M. A. Brzezinski, R. F. Shipe, F. Lipschultz, and M. A. Altabet (1999a), Biological and chemical characteristics of the giant diatom *Ethmodiscus* (Bacillariophyceae) in the central North Pacific gyre, *J. Phycol.*, *35*, 896–902.
Villareal, T. A., C. Pilskaln, M. A. Brzezinski, F. Lipschultz, M. Dennett, and G. B. Gardner (1999b), Upward transport of oceanic nitrate by migrating diatom mats, *Nature*, *397*, 423–425.
Villareal, T. A., R. M. L. McKay, M. M. D. Al-Rshaidat, R. Boyanapalli, and R. M. Sherrell (2007), Compositional and fluorescence characteristics of the giant diatom *Ethmodiscus* along a 3000 km transect (28°N) in the central North Pacific gyre, *Deep Sea Res., Part I*, *54*, 1273–1288.

Wan, S., Z. Yu, P. D. Clift, H. Sun, A. Li, and T. Li (2012), History of Asian eolian input to the West Philippine Sea over the last one million years, *Palaeogeogr. Palaeoclimatol. Palaeoecol.*, *326–328*, 152–159.

Wetzel, F., G. F. de Souza, and B. C. Reynolds (2014), What controls silicon isotope fractionation during dissolution of diatom opal?, *Geochim. Cosmochim. Acta*, *131*, 128–137.

Wischmeyer, A. G., C. L. De La Rocha, E. Maier-Reimer, and D. A. Wolf-Gladrow (2003), Control mechanisms for the oceanic distribution of silicon isotopes, *Global Planet. Change*, *17*, 1083, doi:10.1029/2002GB002022.

Wiseman, J. D. H., and N. I. Hendey (1953), The significance and diatom content of a deep-sea floor sample from the neighbourhood of the greatest oceanic depth, *Deep-Sea Res.*, *1*, 47–59.

Wu, S., T. Ding, X. Meng, and L. Bai (1997), Determination and geological implication of O-Si isotope of the sediment core in the CC area, the Pacific Ocean, *Chin. Sci. Bull.*, *42*, 1462–1465.

Xiong, Z., T. Li, B. Zhai, S. Wan, and Q. Nan (2010), Clay mineral characteristics of *Ethmodiscus rex* diatom mats from low-latitude western Pacific during the last glacial and implications for their formation [in Chinese with English abstract], *Earth Sci. (J. China Univ. Geosci.)*, *35*, 551–562.

Xiong, Z., T. Li, T. Algeo, F. Chang, X. Yin, and Z. Xu (2012a), Rare Earth element geochemistry of laminated diatom mats from tropical West Pacific: Evidence for more reducing bottom waters and higher primary productivity during the Last Glacial Maximum, *Chem. Geol.*, *296–297*, 103–118.

Xiong, Z., T. Li, T. Algeo, Q. Nan, B. Zhai, and B. Lu (2012b), Paleoproductivity and paleoredox conditions during late Pleistocene accumulation of laminated diatom mats in the tropical West Pacific, *Chem. Geol.*, *334*, 77–91.

Xiong, Z., T. Li, and X. Crosta (2012c), Cleaning of marine sediment samples for large diatom stable isotope analysis, *J. Earth Sci.*, *23*, 161–172.

Xiong, Z., T. Li, X. Crosta, T. Algeo, F. Chang, and B. Zhai (2013a), Potential role of giant marine diatoms in sequestration of atmospheric CO_2 during the Last Glacial Maximum: $\delta^{13}C$ evidence from laminated *Ethmodiscus rex* mats in tropical West Pacific, *Global Planet. Change*, *108*, 1–14.

Xiong, Z., T. Li, B. Zhai, and F. Chang (2013b), Quantitative evaluation of paleoproductivity of diatom mats from tropical West Pacific during the Last Glacial Maximum (LGM) [in Chinese with English abstract], *Earth Sci. (J. China Univ. Geosci.)*, *38*, 25–32.

Xu, Z., A. Li, F. Jiang, and F. Xu (2008), Geochemical character and material source of sediments in the eastern Philippine Sea, *Chin. Sci. Bull.*, *53*, 923–931.

Xu, Z., T. Li, S. Wan, Q. Nan, A. Li, F. Chang, F. Jiang, and Z. Tang (2012), Evolution of East Asian monsoon: Clay mineral evidence in the western Philippine Sea over the past 700 kyr, *J. Asian Earth Sci.*, *60*, 188–196.

Xu, Z., T. Li, X. Yu, A. Li, Z. Tang, J. Choi, and Q. Nan (2013), Sediment provenance and evolution of the East Asian winter monsoon since 700 ka recorded by major elements in the West Philippine Sea, *Chin. Sci. Bull.*, *58*, 1044–1052.

Yoder, J. A., S. G. Ackleson, R. T. Barber, P. Flament, and W. M. Balch (1994), A line in the sea, *Nature*, *371*, 689–692.

Yuan, W., and J. Zhang (2006), High correlations between Asian dust events and biological productivity in the western North Pacific, *Geophys. Res. Lett.*, *33*, L07603, doi:10.1029/2005GL025174.

Zhai, B., T. Li, F. Chang, and Q. Cao (2009), Vast laminated diatom mat deposits from the west low-latitude Pacific Ocean in the last glacial period, *Chin. Sci. Bull.*, *54*, 4529–4533.

Zhai, B., T. Li, Z. Xiong, and J. Li (2012), Diatom records inferred from the diatom mat deposits from low-latitude western Pacific in the last glacial period [in Chinese with English abstract], *J. Trop. Oceanogr.*, *31*, 75–82.

Ziegler, K., O. A. Chadwick, M. A. Brzezinski, and E. F. Kelly (2005), Natural variations of $\delta^{30}Si$ ratios during progressive basalt weathering, Hawaiian Islands, *Geochim. Cosmochim. Acta*, *69*, 4597–4610.